Rita Figueiredo Pires

Licenciada em Química Aplicada- Perfil Química Orgânica

Synthesis of Photoactive Dendrimers for Green Photovoltaics

Dissertação para obtenção do Grau de Mestre em
Química Bioorgânica

Orientador: Dr. Vasco Bonifácio, Investigador Principal, IT
Co-orientador: Dr.ª Teresa Casimiro, Investigadora Principal, FCT-UNL

Júri:

Presidente: Prof. Ana Maria Ferreira da Costa Lourenço
Arguente(s): Prof. Doutora Ana Vital Morgado Marques Nunes
Vogal(ais): Doutor Vasco Daniel Bigas Bonifácio

FACULDADE DE CIÊNCIAS E TECNOLOGIA
UNIVERSIDADE NOVA DE LISBOA

Abril 2015

2015

Synthesis of Photoactive Dendrimers for Green Photovoltaics

Rita Pires

Rita Figueiredo Pires

Licenciada em Química Aplicada- Perfil Química Orgânica

Synthesis of Photoactive Dendrimers for Green Photovoltaics

Dissertação para obtenção do Grau de Mestre em
Química Bioorgânica

Orientador: Dr. Vasco Bonifácio, Investigador Principal, IT
Co-orientador: Dr.ª Teresa Casimiro, Investigadora Principal, FCT/UNL

Júri:

Presidente: Prof. Ana Maria Ferreira da Costa Lourenço
Arguente(s): Prof. Doutora Ana Vital Morgado Marques Nunes
Vogal(ais): Doutor. Vasco Daniel Bigas Bonifácio

Synthesis of Photoactive Dendrimers for Green Photovoltaics

Copyrights © belongs to Rita Figueiredo Pires and Faculdade de Ciências e Tecnologia da Universidade Nova de Lisboa.

The Faculdade de Ciências e Tecnologia da Universidade Nova de Lisboa has the perpetual and geographically unlimited right of archiving and publishing this thesis through printed or digital copies, or by any other means known or to be invented, and to divulge its contents through scientific repositories and of admitting its copy and distribution with educational, research, noncommercial goals, as long as its author and editor are properly credited.

Agradecimentos

Antes de mais, tenho que agradecer à Dra. Teresa Casimiro e ao Dr. Vasco Bonifácio pela fantástica oportunidade que me proporcionaram de poder realizar a minha tese de mestrado sob a sua orientação. Obrigada por terem acreditado em mim desde o primeiro dia e por estarem sempre presentes quando precisei.

Vasco, não poderia ter um professor de química orgânica melhor. Sempre cheio de ideias, optimista, nunca baixou os braços nem deixou que eu baixasse os meus quando não obtínhamos os melhores resultados. Para além de todo o conhecimento e técnicas laboratoriais, o Vasco ensinou-me, acima de tudo, a encarar a vida com optimismo e sempre com um sorriso nos lábios, porque por mais problemas que tenhamos, no fim vamos ter um final feliz.

Embora não esteja tão presente na parte experimental, a Teresa foi um pilar fulcral nesta tese, porque esteve sempre presente, a acompanhar o trabalho feito, contribuindo com ideias bastante importantes.

Não posso deixar de agradecer a quem me moeu o juízo durante este ano, o querido colega Zé Jorge. Apesar de seres um chato, estares sempre a gozar com "o tractor da beira baixa" e com os meus maus resultados, sempre que precisei estiveste lá para me apoiar. Tornaste aquele laboratório mais animado e sempre tinha alguém para chatear. Sabes que no fundo, mas bem lá no fundinho eu até gosto de ti.

À minha engenheira/colega preferida na orgânica, a Raquel Viveiros com a sua maneira de ser e o seu sentido de humor põem toda a gente em ordem. Tens sempre uma solução para tudo e és uma óptima conselheira. Para além disso é sempre uma animação estar no laboratório, especialmente quando estás a fazer reacções orgânicas.

Obrigada à Prof. Dr.ª Ana Aguiar-Ricardo por me ter acolhido no seu grupo de investigação em 2013, permitindo que muitas portas se abrissem para mim, e continuar a ser sempre tão carinhosa e disponível mesmo já não sendo sua aluna. À Sofia Silva que tinha sempre uma aventura para contar (aquele dia do sushi em que tentaste passar por deficiente está gravado na minha memória) ao Renato Cabral que estava sempre disposto a ajudar, à Marta Chaves, a minha afilhada linda e que anima os meus dias no laboratório (e sempre com notícias do dia), à Ana Paninho (adoro as nossas conversas ao almoço), e ainda à Catarina Melo, Patrícia Morgado, Vanessa Almeida e a todos os que partilharam o laboratório comigo neste ano, foi fantástico partilhar esta experiência convosco.

A vida não é só trabalho e por isso não poderia deixar de agradecer aos meus amigos, que são poucos mas são os melhores, nomeadamente ao Bruno Lopes (não sei como me aturas à 10 anos), à Vanessa Fadista, Sofia Cardoso, Susana Pulido e Tiago Nunes. Estiveram sempre presentes, ajudam-me quando preciso, apoiam-me nas minhas decisões, ralham comigo quando preciso de ser chamada à razão e acima de tudo, tornam a minha vida muito mais alegre e divertida. Adoro-vos e vão estar sempre presentes na minha vida, porque os amigos da faculdade são para sempre!

Por fim, mas não menos importante, gostava de agradecer aos meus pais do fundo do coração. Nunca me impuseram nada, sempre me deixaram fazer as minhas escolhas e seguir o meu caminho. Sei o esforço que fizeram ao longo destes 5 anos e espero que estejam orgulhosos do meu percurso até aqui e sintam que o vosso esforço foi recompensado. Sou uma pessoa feliz e bem formada graças a vocês.

Resumo

A presente tese de mestrado teve como foco principal a síntese e a caracterização de componentes activos para a produção de uma célula orgânica fotovoltaica baseada com uma matriz de hidrogel (folha artificial).

A síntese de um sistema contendo um dendrímero fotoactivo, um novo sensibilizador de ruténio e de uma β-ciclodextrina "clicável" foi bem sucedido. Este "nanovelcro" será um componente crucial na parte final da construção do dendrímero fotoactivo, mas será apenas usado na construção do dispositivo.

Estudos preliminares de fluorescência e voltametria cíclica foram realizados para as espécies fotoactivas, nomeadamente o PIMAM-OMe_{G1} e o $Ru(dcbpy)_2(NCS)(EAFc)$, com resultados bastante promissores. O PIMAM-OMe_{G1} demostrou capacidade para absorver e emitir luz e ambos têm um potencial redox.

Devido à baixa solubilidade dos dendrímeros fotoactivos em solventes orgânicos comuns e água, o PIMAM-OMe_{G1} sofreu diferentes transformações de modo a melhorar essa solubilidade, embora sem muito sucesso, e, por causa disso, a estratégia encontrada foi usar como matriz um gel iónico em vez de um hidrogel, de modo a permitir a total solubilização das espécies fotoactivas.

Palavras-Chave: Dióxido de carbono supercrítico, Dendrímero fotoactivo, Folha artificial, Célula orgânica fotovoltaica, Orgânica electrónica

Abstract

This master thesis was focused on synthesis and characterization of active components for the fabrication of hydrogel-based organic solar cells (artificial leaves).

The synthesis of a complex photoactive dendrimer and a novel ruthenium sensitizer and the synthesis of a "clickable" β-cyclodextrin were successfully achieved. This "nanovelcro" will be a crucial component of the final photoactive dendrimer unit, and will be used in forthcoming work.

Preliminary fluorescence and cyclic voltammetry studies were performed for photoactive species, PIMAM-OMe_{G1} and $Ru(dcbpy)_2(NCS)(EAFc)$, with very promising results. PIMAM-OMe_{G1} has shown the capacity of absorbs and emits light and both species have a redox potential.

Due to the low solubility of photoactive dendrimers in organic solvents and water, PIMAM-OMe_{G1} suffered several transformations for improving its solubility. Therefore, the final devices were constructed using an ion gel as matrix, instead of a hydrogel.

Keywords: Supercritical carbon dioxide, Photoactive dendrimers, Artificial Leaf, OPV cell, Organic electronics

Contens

Figures

Tables

Abbreviations

BSA – *N*,*O*-Bis(trimethylsilyl) acetamide
[CB]7 – Curcubit[7]uril
β-CD – β-cyclodextrin
CV – Cyclic Voltammetry
DMF – *N*,*N*-Dimethylformamide
DMSO – Dimethylsulfoxide
EAFc – Ferrocene-ethanolamine
FF – Fill Factor
FTIR – Fourier Transform Infrared
HIT – Heterojunction with the intrinsic thin layer
HOMO – Highest occupied molecular orbital
I_{sp} – Short Circuit Current
ITO – Indium tin oxide
LUMO – Lowest unoccupied molecular orbital
MDMO-PPV – Poly[2-methoxy-5-(3′,7′-dimethyloctyloxy)-1,4-phenylenevinylene]
MPP – Maximum Power Point
NMR – Nuclear Magnetic Resonance
OPV – Organic Photovoltaic
PCBM – [6,6]-Phenyl-C_{61}-butyric acid methyl ester
PCE – Power Conversion Efficiency
PEDOT – Poly(3,4-ethylenedioxythiophene)
PEDVD – Plasma enhanced chemical vapor deposition
PH3T – Poly(3-alkylthiophene)
PIMAM – Poly(imidazolone amine)
P_{in} – Incident Light Power Density
P_{max} – Largest Power Output
PSS – Poly(sodium styrene sulfonate)
PUPA – Poly(urea phenylamine)
PURAM – Poly(urea amidoamidine)
PURAP – Poly(urea aminophenyl)
PV – Photovoltaic
SCFs – Supercritical Fluids
$scCO_2$ – Supercritical Carbon Dioxide
Sigma 7-9 – 2-Amino-2-(hydroxymethyl)-1,3–propanediol
TAPA – Tris(4-aminophenyl)amine
TREN – Tris(2-aminoethyl)amine
V_{oc} – Open Circuit Voltage

I. Introduction

a. Purpose of the work

The main goal of this work was the synthesis and characterization of active components for the fabrication of hydrogel-based organic solar cells (artificial leaves). Combining the properties of supercritical CO_2 and organic semiconductors compounds allowed the creation of a complex photoactive dendrimer. Taking advantage of the inclusion capacity of β-cyclodextrin it was possible to create a crucial "nanovelcro" that will link the photoactive dendrimer to a novel ruthenium sensitizer, resulting on a unique system.

This is an exciting new field, which is attracting much interest from the scientific community due to the challenging efficiency improvement of these organic solar cells, one of the biggest disadvantages of this type of devices. To create a low cost, flexible, biocompatible and high efficient artificial leaf using green procedures, such as $scCO_2$-assisted polymerization, was our purpose and big challenge.

b. Green chemistry

Since the beginning of the development of the chemical industry, serious environmental issues, such as pollution, risk of fire or explosions, caused by this sector become a world concern [1].

In this sense, green chemistry is a concept that is increasingly becoming assumed by the scientific community, especially in the last two decades. There are many definitions for green chemistry, but they all lead to an idea towards a cleaner chemistry without compromising the target goals, either the synthesis or the reactions efficiency [2]. In 1991, Paul Anastas introduced the first definition to the scientific community, creating in 1998 with John C. Warner, from the United States Environmental Protection Agency, " The Twelve Principles of Green Chemistry" [3] to help the scientific community to understand how they can apply this concept on practice. These principles are as follow:

I. Prevention

It is better to prevent waste than to treat or clean up waste after it has been created.

II. Atom Economy

Synthetic methods should be designed to maximize the incorporation of all materials used the process into the final product.

III. Less Hazardous Chemical Syntheses

Wherever practicable, synthetic methods should be designed to use and generate substances that possess little or no toxicity to human and the environment.

IV. Designing Safer Chemicals

Chemical products should be designed to affect their desired function while minimizing their toxicity.

V. Safer Solvents and Auxiliaries

The use of auxiliary substances (*e.g.* solvents, separation agents) should be made unnecessary wherever possible and innocuous when used.

VI. Design for Energy Efficiency

Energy requirements of chemical processes should be recognized for their environmental and economic impacts and should be minimized. If possible, synthetic methods should be conducted at ambient temperature and pressure.

VII. Use of Renewable Feedstocks

A raw material or feedstock should be renewable rather than depleting whenever technically and economically practicable.

VIII. Reduce Derivatives

Unnecessary derivatization (use of blocking groups, protection/deprotection, temporary modification of physical/chemical processes) should be minimized or avoided if possible, because such steps require additional reagents and can generate waste.

IX. Catalysis

Catalytic reagents (as selective as possible) are superior to stoichiometric reagents.

X. Design for Degradation

Chemical products should be designed so that at the end of their function they break down into innocuous degradation products and do not persist in the environment.

XI. Real-time Analysis for Pollution Prevention

Analytical methodologies need to be further developed to allow for real-time, in-process monitoring and control prior to the formation of hazardous substances.

XII. Inherently Safer Chemistry for Accident Prevention

Substances and the form of a substance used in a chemical process should be chosen to minimize the potential for accidents, including releases, explosions and fires.

In this work we followed many of these principles, such as I, II, III, IV, VII or VIII and always tried to use the small amount possible of solvents, looking for efficient and clean alternatives. One of the biggest problems in chemicals processes is the use of organic solvents, usually toxic, flammable and volatile. They are also frequently responsible for waste generated during a given process, especially if that process involves many purification steps, since frequently they are not incorporated into the final products and, in spite of they could be recycled, most often them are lost to environment or required to be disposable as waste [1,4,5].

Aiming to avoid these problems, scientists have been looking for alternatives to organic solvents that could minimize the environmental impact. Therefore, alternative solvents able

reduce the energy consumption and produce less toxic residues, such as the use of water, "renewable" solvents derived from biomass, ionic-liquids or supercritical fluids, are being employed [4,6].

i. Supercritical Fluids

A supercritical fluid is a state of a compound or a mixture above its critical pressure (p_c) and temperature (T_c), but below the pressure to condensation. As shown in Figure I.1 when the compound reaches is critical point it is just possible to observe one single phase (see Figure 1.1 c).

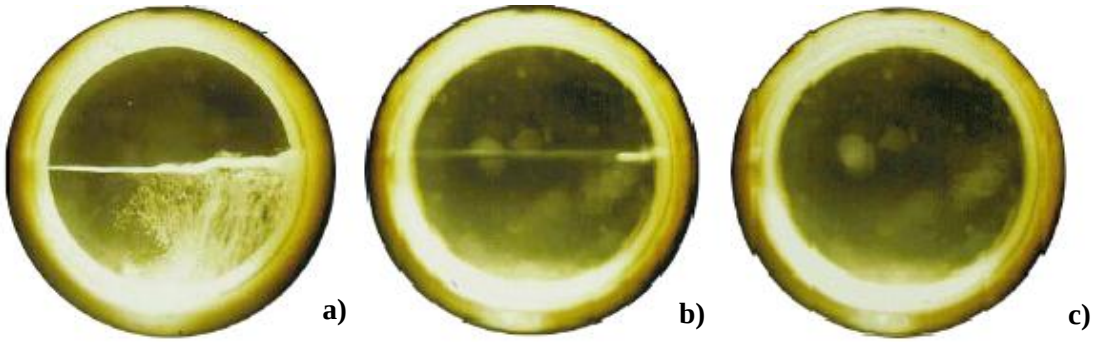

Figure I.1: Visual observation of the stages until formation of a supercritical fluid: pictures a) and b) show the liquid-gas equilibrium ($T<T_c$) and picture c) show the supercritical fluid ($T\geq T_c$). This experience was performed heating the substance above its critical temperature with a pressure higher than its critical pressure. Adapted from references [1,7,8].

Discovered in 1822 by Cagniard de la Tour [7], SCFs shows unique physicochemical properties such as the special combination of liquid-like density and solvating properties and gas-like viscosity and diffusivity. Therefore, SCFs are excellent solvents, also more sustainable, environmentally friendly and with low cost. They have easily tunable solvating power which enable the control of the reactivity and the selectivity of the reaction. That is one of the reasons for the growing use of SFCs in many reactions, such as hydrogenation or enzymatic hydrolysis for example [6,8].

Table I.1: Critical Temperatures and Pressures of solvents used as SCFs [8,9].

Solvent	Critical Temperature (K)	Critical Pressure (MPa)
Carbon Dioxide (CO_2)	304. 15	7.38
Water (H_2O)	647.35	22.06
Ethane (C_2H_6)	305.35	0.203
Propane (C_3H_8)	369.85	0.217
Ethylene (C_2H_4)	262.45	0.215
Methanol (CH_3OH)	513.15	0.272
Ethanol (C_2H_5OH)	516.25	0.276
Acetone (C_3H_6O)	508.05	0.278

There are many solvents that could be used as SCFs and used in different processes, such as extraction, organic synthesis, catalysis, polymerization, impregnation, morphological modifications, dry cleaning, high pressure sterilization, thin film deposition on microelectronics, jet cutting or supercritical fluid chromatography [6,10]. SCFs have been used in so many industrial processes once a process involving SCFs require less energy and is environmentally friendly compared to organic solvents, and besides that, the unique properties of SCFs turns this process more and more attractive to industry [6]. In spite of this variety of SCFs, CO_2 is one of the most used solvents as SCFs, not only for its low critical point but also for its properties.

ii. Carbon Dioxide

Known for being a greenhouse gas, the emission of CO_2 is the biggest contributor to global warming as it shown on Figure I.2a. The rising values of CO_2 emissions, caused mainly by the burning of fossil fuels, provided from energy supply and industry, and also the harvesting of forest in the tropics (Figure I.2b) [11], became a serious problem that concerns the world since has a tremendous effect in climate changes [12].

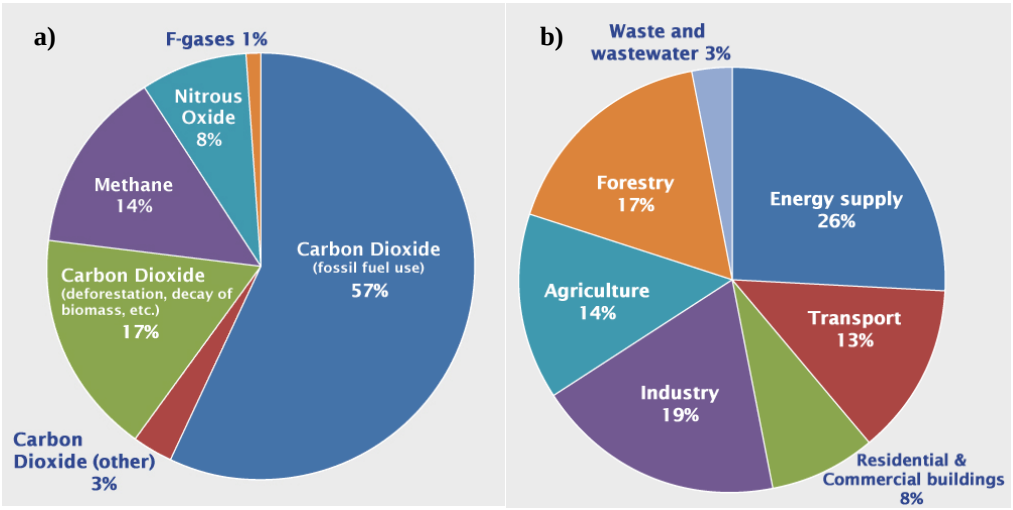

Figure I.2: Global greenhouse gas emission by gas (a) and by source (b) [12].

Therefore, new technologies are being developed to stop and diminish this serious problem. Besides, to reduce the consumption of carbon-based fuels (fossil fuels) and start using carbon-free energy sources, the alternatives founded were the capture of CO_2 from power plants. This can be done by removing it from atmosphere and retaining it (store) within plants and soil, or capturing it (either before or after fossil fuel is burned) and then it can be stored (sequestered) within earth [11].

With the continuous growing interest of using SCFs by the industry in the last decades [7], CO_2 has aroused much attention in this area, being also designed as an green solvent in 2005 by Noyori [5]. Having an easily accessible critical point (Figure I.3), and being non-toxic, non-flammable, environmentally acceptable, relatively low cost, readily available (is a sub-product from industry), chemically inert under many conditions, thermodynamically stable and with particular solvating properties [4,12], nowadays CO_2 is one of the most used supercritical fluids.

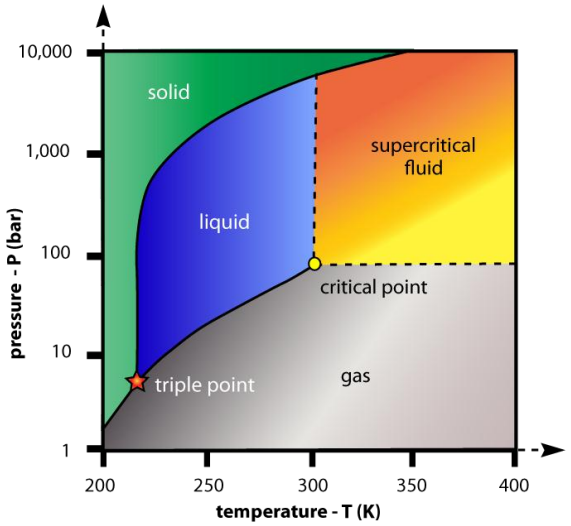

Figure I.3: Carbon dioxide pressure-temperature phase diagram [13].

There are many applications that use $scCO_2$. One of the most popular is coffee decaffeination [4]. The unique properties of $scCO_2$ (*e.g.* diffusivity approaching of a gas combined with the solvent power of a light liquid alkane or its power of solvation for nonpolar materials) turn $scCO_2$ an attractive alternative solvent in some reactions such as hydrogenation (using H_2) or oxidation (with O_2), thus promoting high levels of selectivity in some reactions [4,8].

In the pharmaceutical field, $scCO_2$ became also very important, since the use of $scCO_2$ allows the control of size, morphology and impregnation efficiency of the drugs [14]. The fact that CO_2 is nontoxic, nonflammable and inexpensive is besides a great advantage over common organic solvents.

The polymerization reactions using $scCO_2$ have been also growing in the last years. For example, Christian *et al.* [15], Casimiro *et al.* [16] and Macedo *et al.* [17] described successful free-radical or cationic ring-opening polymerizations using $scCO_2$. Furthermore, crosslinking reactions are very successful in $scCO_2$, and several examples can be found in literature [18,19]. The incorporation of CO_2 molecules in the polymers backbone during the synthesis was also described by Restani *et al.* [20]. Interestingly, in this case $scCO_2$ was used not only as solvent, but also as a reagent.

All these peculiar characteristics and different uses make $scCO_2$ an attractive solvent for industrial applications.

c. Fossil Fuels

Coal, natural gas and oil are designed as fossil fuels. Composed by hydrocarbons, fossil fuels are formed by natural processes such as the anaerobic decomposition of buried dead organisms. Briefly, like is shown in Figure I.4, after dead of forests (in case of coal) or marine

plants and animals (in case of oil and gas), they are buried and compressed into layers of sediments, several kilometers below the ground. With pressure and temperature conditions that are verified inside Earth, bacteria convert biomass into precursor substances from which hydrocarbons, originate coal, oil or natural gas. These transformations are very slow, and usually it takes around 300 million years until the process is complete, but sometimes it could reach 650 million years [21,22,23].

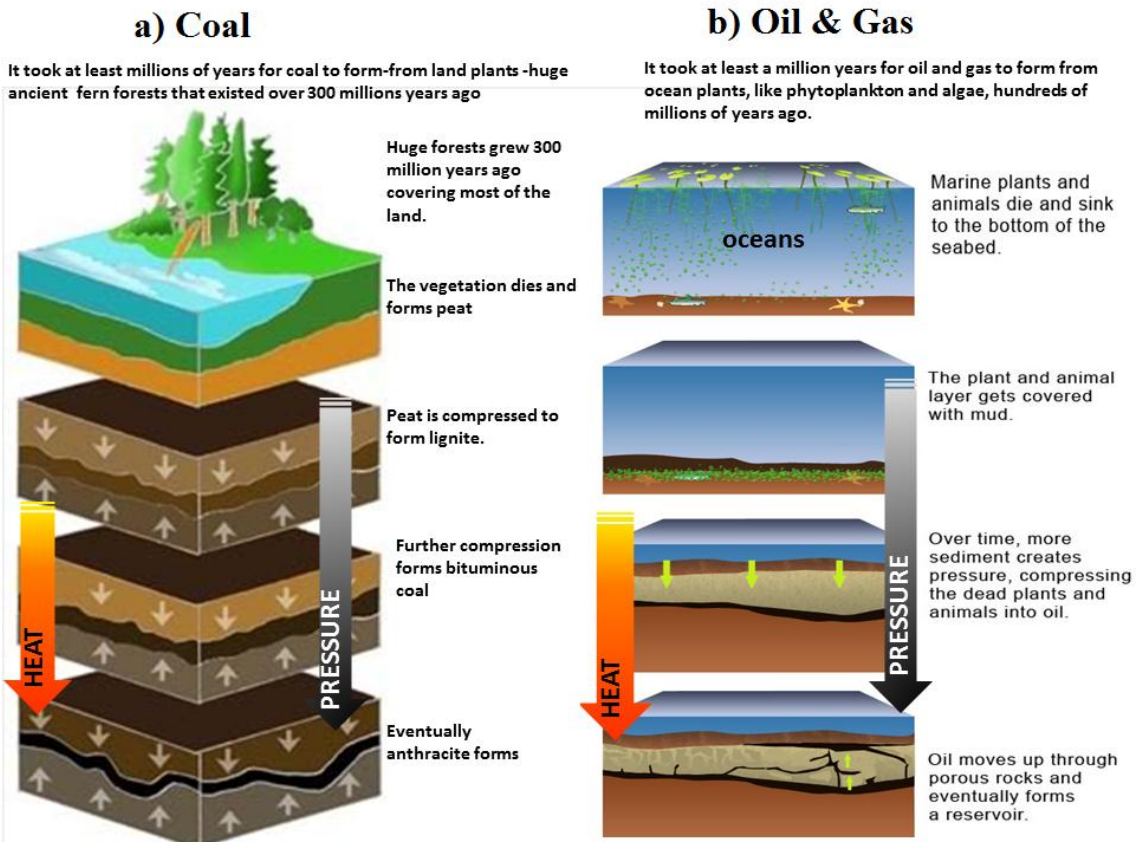

Figure I.4: Formation of fossil fuels: a) formation of coal and b) formation of oil and gas [23].

Until the industrial revolution in the 1700s, the use of fossil fuels was not common, in spite of coal, known since pre-history and used for heating purposes since that time. With the industrial revolution the world started developing and new discoveries, such as artificial lighting, the evolution of transportation or industry development, led to an huge demand of energy production [24,25]. Actually, most of the global energy consumption is provided from fossil fuels burning (around 77.9%), as described in Figure I.5. This raises serious environmental concerns, once during fossil fuels burning CO_2 is released to the atmosphere. As it was previously stated (see Figure I.2a), CO_2 is a greenhouse gas, and *ca.* 57% of the CO_2 emissions came from fossil fuels burning. Also, although fossil fuels are being continually formed via natural processes, they are considered a non-renewable resource, once they take millions of years to form and with our actual lifestyle, especially on developed countries, the

viable reserves are being depleted much faster than new ones are being created, which can lead to their disappearance in the forthcoming decades.

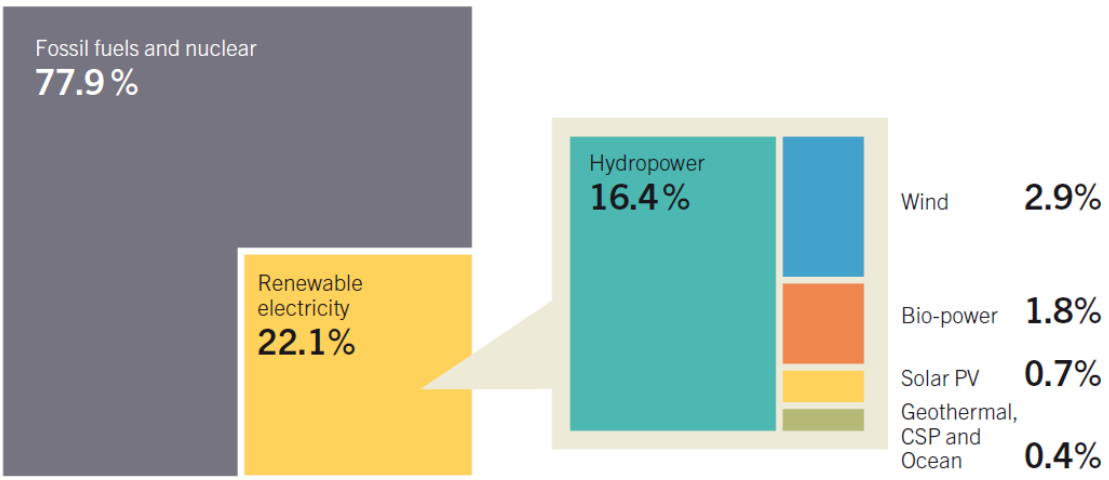

Figure I.5: Estimated energy shared of global electricity production in 2013 (based on renewable capacity in operation in 2013) [26].

d. Renewable Energy

In 1970s the world suffered the first oil crisis [27]. This crisis increased extremely the oil price. Being a resource that is in extinction and with a price increasingly higher, an urgent search for new energy production alternatives was initiated, especially for solutions that could be benign to the environment and be able to support a sustainable lifestyle.

Under this context, renewable energy emerged as an alternative solution. This energy is defined as the energy that is derived from natural processes (*e.g.* wind or sunlight) that are replenished at higher rate than its consumed [28]. Over the past decade the global perception of renewables shifted considerably, and with continuing technology advances have shown their immense potential. Moreover, they became not only an alternative source of energy, but also a tool to address many other pressing needs including: improvement of energy security, reduction of the health and environmental impact associated with fossil fuels, mitigation of greenhouse gas emissions, promotion of economic development (improvement of educational opportunities, creation of jobs, reduction of poverty and increasing of gender equality) [26,28].

In spite of the consumption of renewable energy being still be very low (only 22.1%), as it is possible to observe in Figure I.5, the tendency is for a growth in the next years, once the technology used is more sophisticated and more efficient. In Figure I.6 it is possible to observe the different types of renewable energy resources, depending of the natural source used.

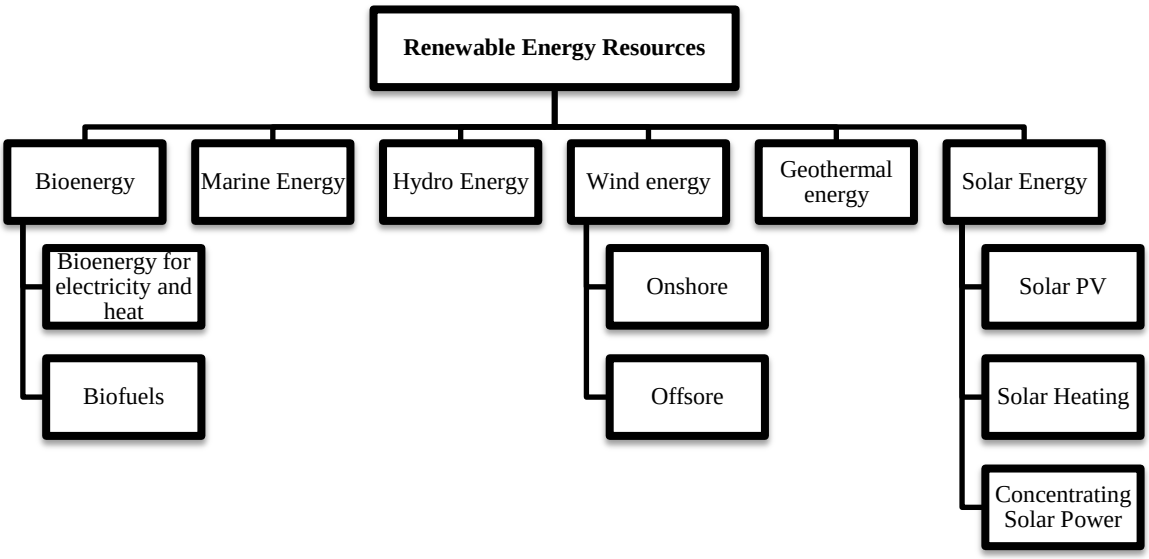

Figure I.6: Overview diagram of renewable energy sources [29].

i. Bioenergy

Used to produce electricity, warming of buildings and water, industrial processes, or formation of liquid fuels (biofuels), bioenergy is the energy provided from the conversion of biomass, defined as any organic matter derived from animals or plants (*e.g.* wood, charcoal, agricultural crops, municipal organic wastes or manure) [28,29].

Similarly to fossil fuels, but being sustainable and renewable, biomass can be directly burned in order to produce energy, or could be converted into various liquid or gas fuels [29].

The biggest advantage of this type of energy is the reutilization of waste and the production of biofuels that can be transported and stored, and allow heat and power generation. However the associated low energy density and collection and transportation implies high cost and some environmental threats (*e.g.* reduced biodiversity due to soil pollution) [29].

ii. Marine Energy

The ocean can provide energy from waves, tidal currents, ocean currents and ocean thermal energy conversion and salinity gradients. Despite the innumerous ways of using ocean to product energy, the technology conversion of this source is still been developed, being one of the reasons for low adhesion to marine-based energy. Yet some countries like Portugal have been investing this type of energy [28,29].

iii. Hydro Energy

From the renewable energy options, hydro energy is the most used to produce electricity (16.4% in 2013) as it was shown in Figure I.5. Water flowing in turbines creates energy that can

be captured and converted into electricity. This energy can be collected through a run-of-river hydropower plant (using the flow of the river), a reservoir hydropower plant (relies on stored water in a reservoir) or *via* pumped storage plants (use of water that is pumped into an upper reservoir) [28,29].

The advantages of this renewable energy are the abundance of this natural resource, the fact that this is a clean, relatively inexpensive and safe process, and it is very easy to store it in reservoirs. However, the infrastructures can cause a significant environmental impact because of the potential flooding of surrounding communities and landscapes. Also it can be only used where there is a water supply, and the best sites for dams have already been developed, so the development in this area is not so big as the one observed with other sources [28,29].

iv. Wind Energy

Through wind turbines it is possible to convert the kinetic energy of the wind into electricity. This technology has been improved since the beginning of the oil crisis, making possible the implementation of wind farms not only onshore but also in the sea (offshore), becoming one of most important sustainable energy resources [28,29].

It is a free source of energy that does not produce even water or air pollution, with the relatively low cost of wind farms installation, this renewable energy still have some week points once requires constant and significant amounts of wind, the wind farms require considerable amounts of land, causing a significant visual impact and the technology of energy storage needs to be improved [28,29].

v. Geothermal Energy

Reusing the internal energy from Earth its possible to produce electricity, heating or cooling water using different technologies. It is considered a cost effective, reliable and environmental energy source, but the star-up/development and maintenance costs can be expensive. Besides, its a resource that is more efficient in regions with active volcanoes, and consequently is not accessible to all [28,29].

vi. Solar Energy

The sun is a natural resource that will be a source of energy for billions of years. It could be used for electricity production, through PV cells and concentrating power systems or for heating water via solar thermal systems [28,29].

The biggest advantages of this renewable source are the fact that the sun is almost a potentially infinity energy supply and does not cause neither water or air pollution. However may not be cost effective, its necessary to storage and backup and the reliability depends on availability of sunlight [28,29].

e. Solar Photovoltaic Cells

In the last years solar power received a huge global investment, thus promoting the development of new technologies with lower cost and higher efficiency. In spite of a lower global investment in 2013 (less 20%, see Figure I.7), a new record of installation was verified in 2013, and consequently a new record on solar PV capacity (Figure I. 8) [26].

The first type of studied PV cells was inorganic solar. However, nowadays we found also a great interest for organic and hybrid organic-inorganic solar cells.

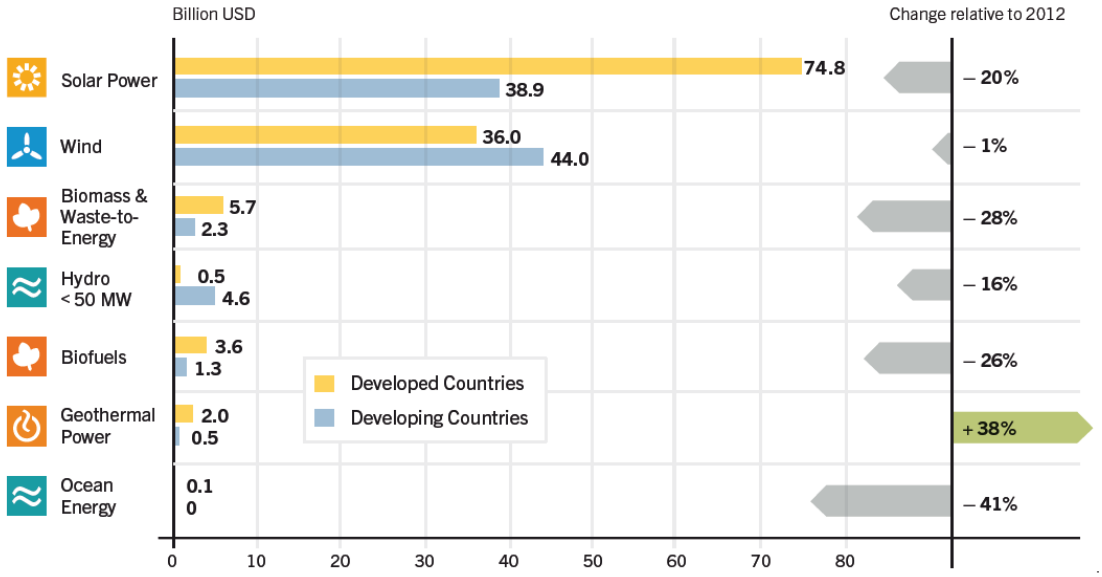

Figure I.7: Global investment in renewable energy by technology in 2013 [26].

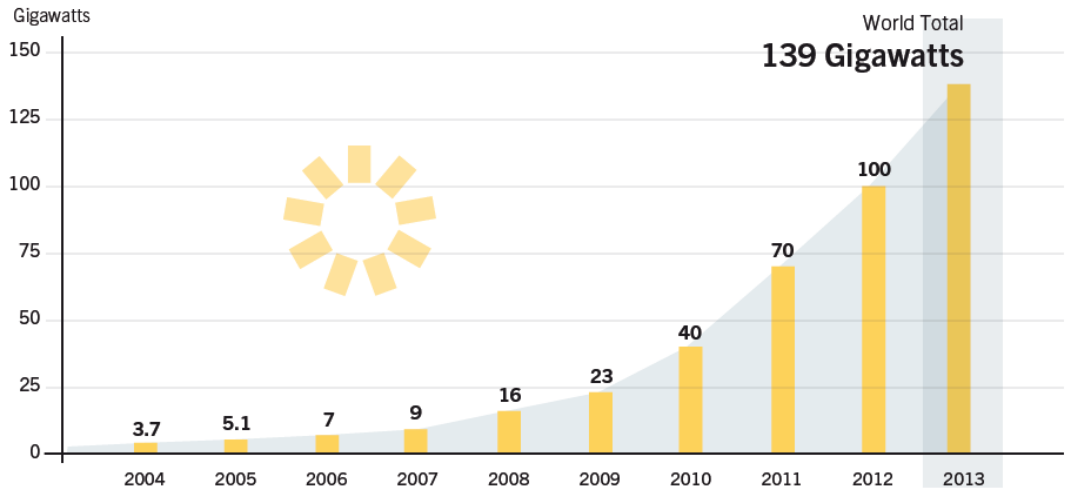

Figure I.8: Solar photovoltaic total capacity in the period 2004-2013 [26].

i. Inorganic Photovoltaic Cells

The photovoltaic energy revolution started in 1954, the year when the photovoltaic effect in silicon diodes was discovered [30]. Environmentally safe and very abundant on Earth (26% of crustal material), silicon became an attractive material for industry [31]. The phenomenon involved behind the production of electricity from sunlight is known as "light-generated current" [32]. Firstly, the incident photons are absorbed creating an electron-hole pairs within the semiconductor material (*e.g.* silicon). Inside the cell, there are two different types of silicon: n-type, which has square, and the p-type (with boron atoms), which is missing electrons, leaving "holes" in their place. They are disposed side by side into the cell creating an electric field, once the p-type silicon becomes negatively charged and the n-type silicon becomes positively charged when the n-type silicons's square electrons jump to over fill the gaps in the p-type silicon (Figure I.9) [33,34].

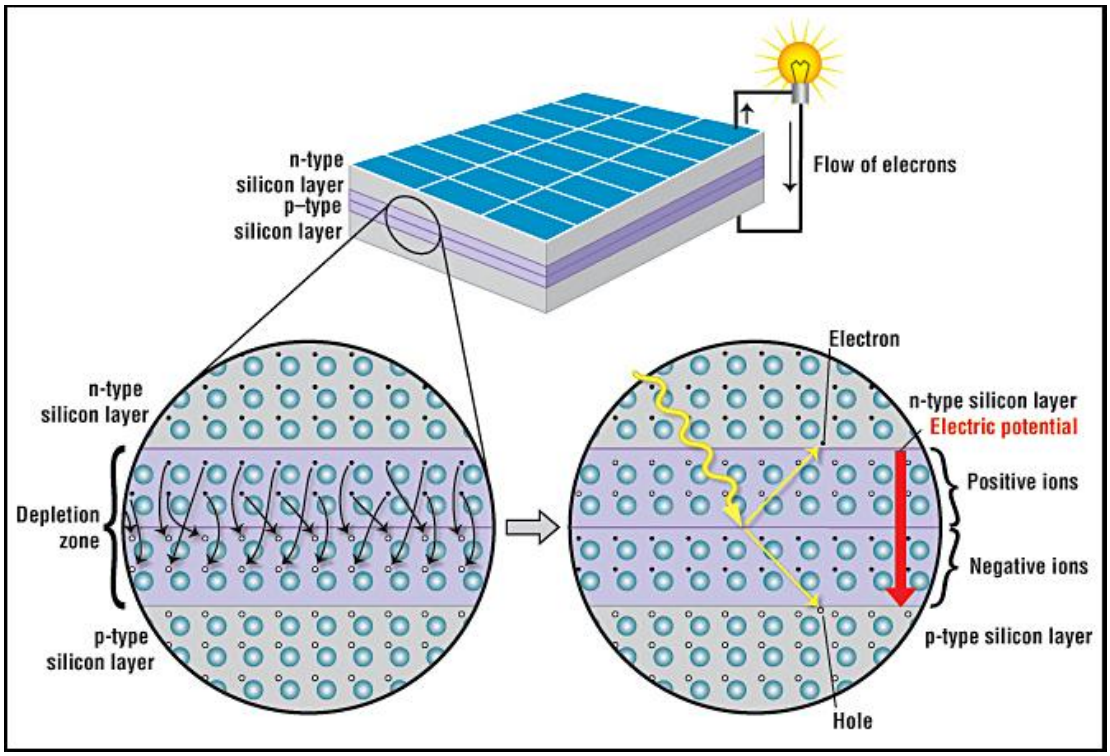

Figure I.9: Schematic representation of an inorganic solar cell, with a close-up view of the depletion zone around the junction between the p-type and n-type layers [34].

Over the past few years, inorganic solar cells have been improved by producing new materials (*e.g.* CdTe) to reduce not only the size but also the price of photovoltaic devices, the two major barriers for the implementation of solar energy in the market. Presently, the available inorganic solar cells are Silicon-based cells, III-V solar cells and thin-film solar cells based on semiconductors [35].

Silicon-based cells

In the Si-based cells category are included crystalline, polycrystalline and amorphous Si, and HIT solar cells.

Crystalline Si is the most popular cell type and the one who suffered a fast growth on the PV market (44% between 2000 and 2013) [31,36]. These PV cells are produced from pseudo-square silicon wafer substrate cut ingots by the Czochralski process; a method of crystal growth used to obtain crystals of semiconductors, such as silicon, with high purity [32]. Crystalline Si has an ordered crystal structure. Combining the predicted and uniform behavior of Si, a well-defined structure is produced (Figure I.10), where each silicon atom has four electrons in the outer shell [32].

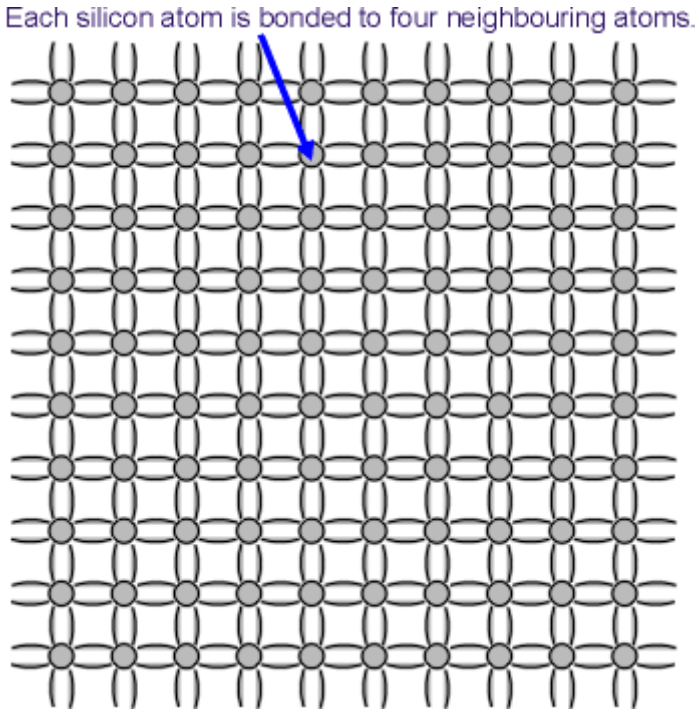

Figure I.10: Rearrangement of a crystalline Si wafer [32].

This type of cells has an indirect energy band gap causing a low optical absorption coefficient, being the reason why the wafer size is so high (more than 200 μm thick). Trying to minimize the refection losses, these cells are "textured" with a solution of NaOH and isopropyl alcohol. The p-n junction is made by diffusing phosphorous into the wafer as an impurity dopant [35].

As can be seen in Figure I.11, the usual crystalline Si solar cells have a screen-printed silver (Ag) contact fingers on the n-type surface to make electrical contact while also allow light to be transmitted to the junction region and an aluminum (Al) is used to make the contact with the back p-type surface. A p^+ doped region is created to lower the contact resistance and provide a back surface field [31,35].

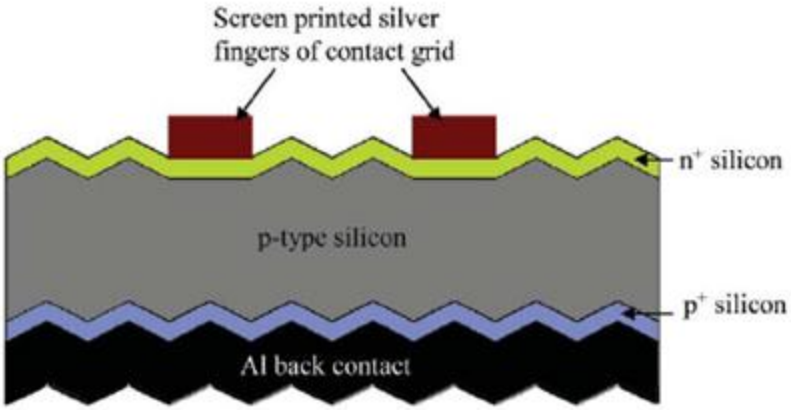

Figure I.11: Cross-sectional view of an crystalline Si cell [35].

In spite of having relatively good efficiency (*ca.* 24.7%) its cost is very high, once the materials need an high purity level and the cell and modulation process is also expensive [31,35].

Other type of Si based cells that suffered a considerable growth on the last years, becoming the most used PV cells in industry (55% of the PV production in 2013), are the polycrystalline Si solar cells [36].

Polycrystalline Si solar cells are easier to produce then crystalline Si solar cells and are cheaper, however, the quality of the material is lower, due to the presence of grain boundaries (Figure I.12), which introduces high-localized regions of recombination, reducing the global minority carrier lifetime of the material. These grain boundaries unfortunately reduce the solar cell performance by blocking carrier flows and allowing shunting paths for current flows across the p-n junction [32].

The conventional method for the production of these cells is using PECVD to deposit silicon nitride as the top insulating layer, instead of SiO_2, as hydrogen is used in this process. Otherwise, the cell process is similar to that used for crystalline Si solar cells and, in spite the efficiency of this type of cells is less than 2-3% in relation to crystalline Si solar cells, the cost is only 80% of crystalline Si solar cells production, being one of the reasons of the biggest growth on the market on the last years [35].

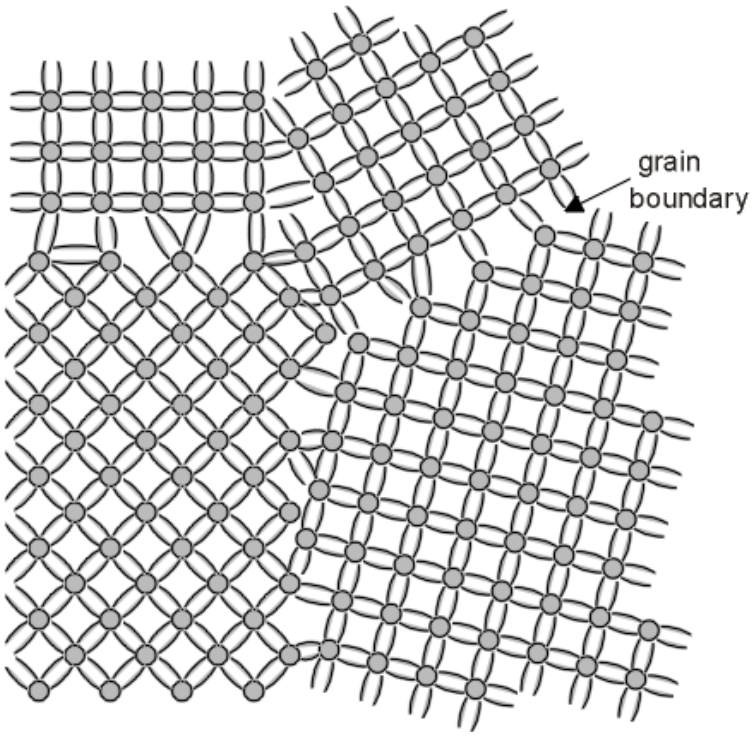

Figure I.12: Schematic representation of a polycrystalline wafer [32].

Amorphous Si solar cells have been aroused some interest on last few years. Produced like polycrystalline solar cells, but using PECV of gases containing silane. The layers could be deposited onto both rigid (*e.g.* glass) or flexible (*e.g.* metallic sheets and plastics) substrates and the material used is hydrogenated amorphous [35]. The presence of hydrogen is very important, because it has an important role of passivating the dangling bonds resulting on a random arrangement of the Si atoms allowing the absorption of most of the incident light with just a few microns of material, reducing the materials and cost of production [35]. The biggest problem is the low efficiency compared with the polycrystalline an crystalline Si solar cell (only 10%) because of the Staebler-Wronski effect (light-induced metastable changes in the properties of hydrogenated amorphous silicon) [35,37].

The last types of Si solar cells are HIT solar cells. In this case, the layers of amorphous Si are deposited onto both faces of a textured wafer of crystalline Si, resulting on a device with better efficiency than the amorphous Si solar cells (around 17.3% in modules). Also, the fact of having a good surface passivation and a low-temperature processing gave them bigger advantages since it is possible to reduce the energy packing time and the relative cost [35].

III-V solar cells

This type of cells involves new inorganic compounds, such as GaAs, InP, GaSb, and it is possible to have single- or multiple-junction solar cells [35].

These materials have direct energy band gaps, good values of minority carrier lifetime and mobility and high optical adsorption coefficients, becoming excellent high efficient materials [35].

The single-junction solar cells are commonly made by the liquid – encapsulated Czochralski method (based on the Czochralski method but the melt is isolated from air by a layer of molten boron oxide, being one of the reasons for the presence of boron as a contaminant) or by the Bridgman method (similar to the Czochralski method but here a temperature gradient is created along the length of the crucible) and GaAs and InP are the most used compounds, showing conversion efficiencies around 25.8% and 21.9% respectively [35,38]. The biggest disadvantage is the high cost of production, once high purity crystals are needed to obtain the high efficiencies [35].

With multi-junction solar cells the losses of solar energy can be reduced getting efficiencies of 30% in GaAs/GaSb stacked cells for example. This is an area still in developing but very promising [35].

Thin films solar cells based on compound semiconductors

In these types of cells, CdTe is the predominant component and the system CdS/CdTe is the one that shows higher efficiency. The production of this type of solar cells is represented on Figure I.13. The need of lower amounts of components to produce these types of devices reduces in large scale the price of the cells production, without compromising the efficiency, once this devices could reach a 16.5% of efficiency [35].

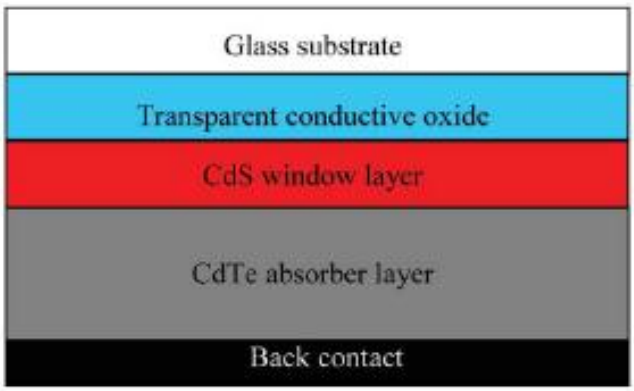

Figure I.13: Representation of a CdS/CdTe thin-film solar cell [35].

Other system that has been attracting much interest is the system using copper. Initially just systems with copper, indium and selenide (CIS) were produced, but rapidly gallium was introduced onto this systems because it was verified that led to an improvement of the efficiency, and the system produced ever since was a solid solution containing copper, indium, gallium and selenide (GIGS) [35].

The best GIGS device produced so far, with efficiencies around 19.5% on laboratory, is shown in Figure I.14. Here the clack contact is made by a thin-film of Mo deposited by a magnetron sputtering. After that, the GIGS absorber layer is formed (it could be by coevaporation of the elements either uniformly deposited or using a metallic precursor layer and made the selenization and/or sulfidization). For the window layer the best material founded until now is CdS and for buffer layer ZnO has been found to be the best material to prevent any shunts. For the transparent conductive oxide ZnO:Al is commonly used. Finally, a metal grid of Ni/Al is deposited for current collection [35]. This type of devices have been intensively studied on last few years trying to improve the efficiency and find new materials to reduce the cost production without compromising the energetic efficiency.

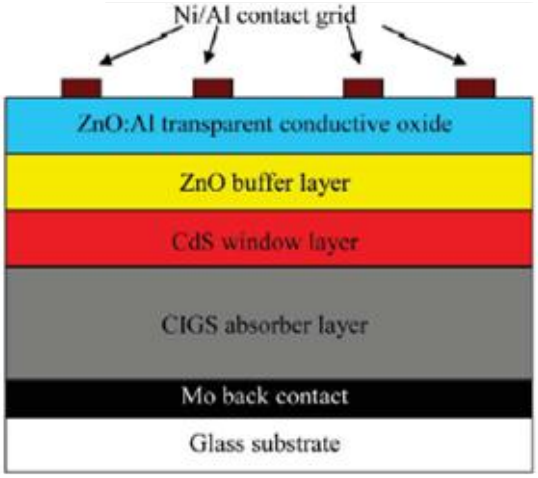

Figure I.14: Representation of a CdS/GIGS thin-film solar cell [35].

ii. Organic Solar Cells

A few years ago the emerging of a new class of PV based on organic materials emerged and made a revolution into the PV market. The materials became a promising alternative to inorganic solar cells, mainly because of their peculiar advantages such the low cost, easily production, using techniques such spin coating (creation of a thin film by centrifugal force), doctor blade techniques (wet-processing) or evaporation through a mask (dry-processing). The fact that only a small amount of material is needed makes the production in large scale much easier in comparison with inorganic materials. Also, a large range of organic compounds can be explored turning these devices highly versatile [30,39]. The only problem associated with OPV devices are the low PCE, currently around 10% [30]. Therefore, improving efficiency has been one of the driving forces on OPV cells research, trying to develop new strategies to improve these devices.

One of the reasons that makes OPV cells so interesting is the fact that practically any organic semiconductor could be used as potential material. By definition, a semiconductor is any compound that has a conjugated system based on π electrons, allowing jumps from site to site between carbon atoms without requiring much energy like the one is needed for ionization. The energy space (band gap) between bounding and antibounding π molecular orbitals, namely the HOMO and LUMO orbitals, is most important feature in terms of electronic properties, once it makes possible the absorption of the light, the creation of photogenerated charge carriers and its transport [39-41].

The diversity of materials that can be used for these solar cells is enormous. It is possible to use polymers, oligomers, dendrimers, organo-minerals, dyes, pigments and many other compounds. Besides semiconductive properties it is also possible to take advantage of the unique properties of each one, such as the valence and conduction energies, the charge transport, as well as the solubility [39]. For example, polymers have a number of identical repeat units, all linked together in a linear way. Deposited by wet process, they could be very soluble in different solvents or insoluble, could be attached together (crosslinked) and usually are used in a glassy state. On the other hand, as an example, if we choose pigments, these small molecules have specific important properties for light absorption and charge generation and the way of processing is usually made by sublimation and the pigment thin films are polycrystalline [39].

In Figure I.15 are represented some organic semiconductor materials that have been used for the construction of OPV devices. Such as for inorganic solar cells, OPV cells also need a donor and acceptor species (*n* and *p* type respectively).

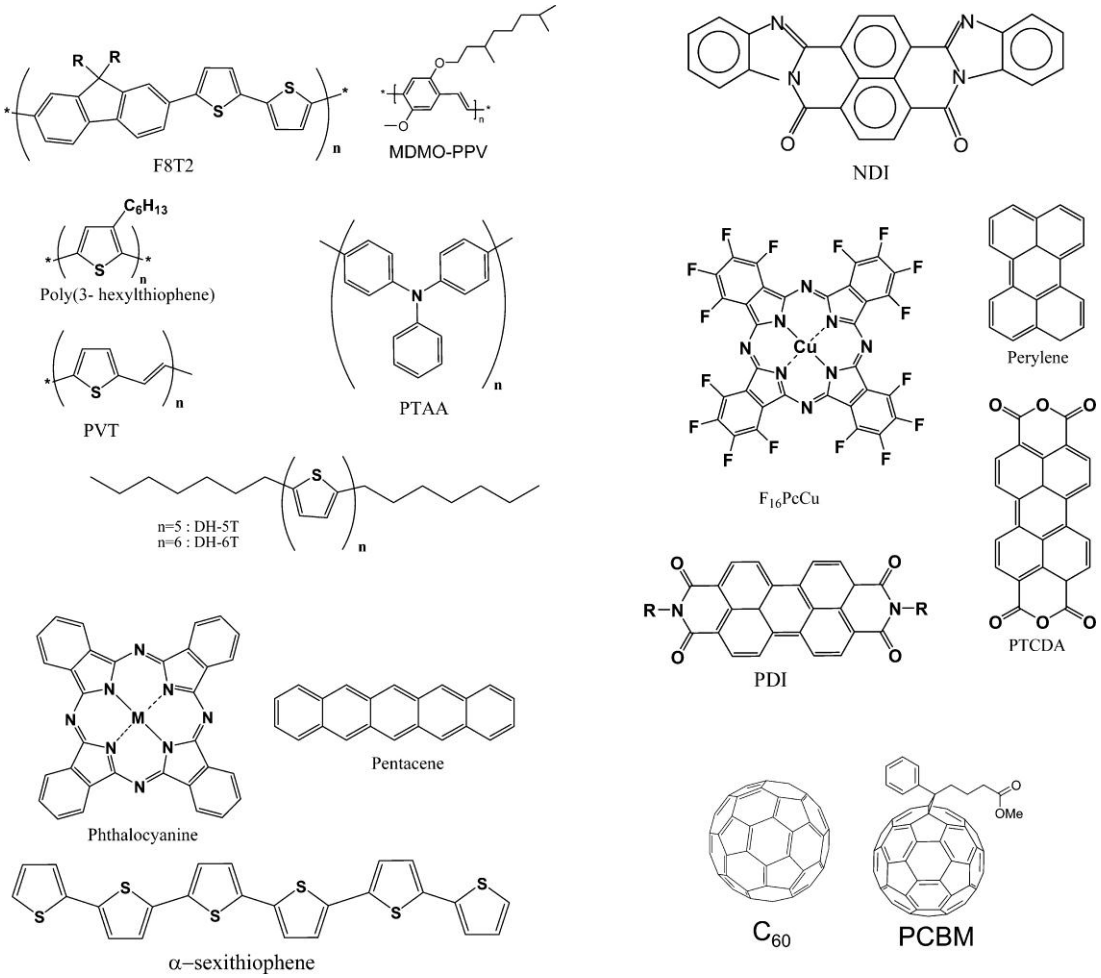

Figure I.15: Representation of some organic semiconductors materials used in OPV devices [40].

The production of current using OPV cell begins with the generation of carriers when the incident photoelectrons excite the donor (an electron goes from the HOMO to the LUMO level), and after that the electron is transferred to the acceptor. Then the carriers are collected by the electrodes and driven to the external circuits. This process is illustrated in a chosen example shown in Figure I.16a and Figure I.16b, where charge generation is obtained using a PPV polymer (donor species) and C_{60} (acceptor species) [39,40].

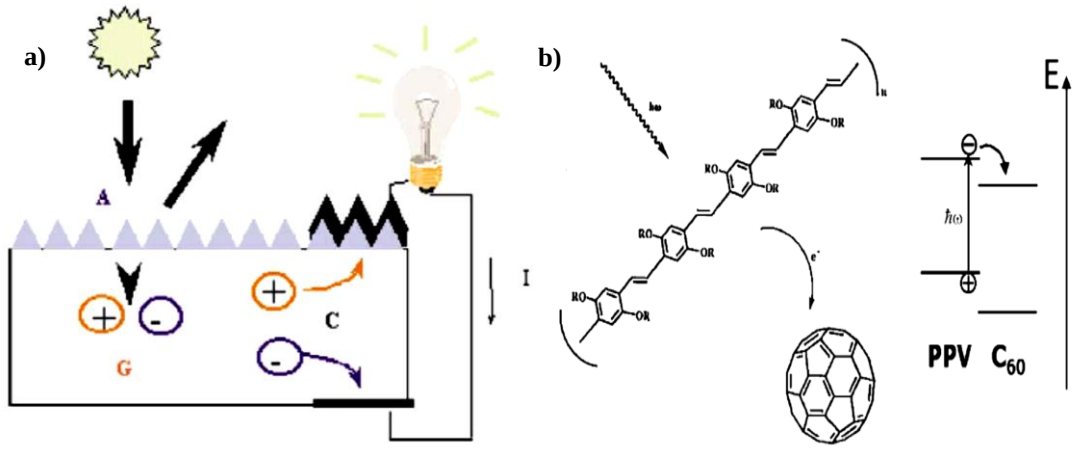

Figure I.16: Operation of an OPV cell a) with representation of the photovoltaic process: (A) absorption of photons, (G) generation of carriers and (C) collection of carriers. Schematic representation b) of a photoinduced charge transfer when the donor species (PPV) is excited by the photon and the electron transferred to the acceptor species (C_{60}) [39,40].

Generally, OPV devices are fabricated using a sandwich geometry and in order to have the specific requirements for efficient photon to charge conversion, different device architectures have been developed. Currently is possible to find single layer, bilayer and also bulk heterojunction devices.

Single Layer Devices

Single layer devices are the simplest OPV systems. Fabricated with a sandwich type architecture (as shown in Figure I.17), the transparent, conducting electrodes are used as substrates, that are usually glass or plastic covered with ITO. In spite of ITO electrodes being transparent and conductive they are expensive and some alternatives has been investigated to find less expensive materials such carbon nanotubes [40,42]. Using the deposition techniques above mentioned the active layer is coated and, finally, the top electrode is evaporated, using, normally, Aluminum, Magnesium or Calcium (usually is used a lower work- function metal that ITO) [39,41,43].

The difference between the HOMO levels of the two conductors, electron will flow from the low-worker function metal (*e.g.* Aluminum) to the lowest-worker function metal (*e.g.* ITO) until they reach the same chemical potential generating an electric field across the semiconductors and when he absorbs the light generates a current and a voltage [39,43].

The disadvantage of these cells is the fact that, in practice, they do not work well because of the exciton phenomenon (the photoexcited electron is electrostatically bound to the hole left in the valence band) [39,43].

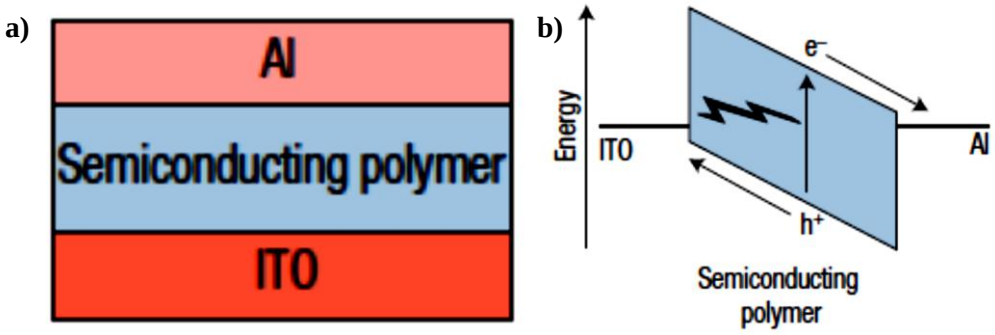

Figure I.17: Representation of a model a) and a schematic energy band b) of a single-layer semiconductor – polymer solar cell [43].

Bilayer Devices

In order to avoid the problems verified on single layer junction devices, in bilayer devices a second semiconductor is incorporated, therefore p-type and n-type layers are sequentially stacked on top of each other (Figure I.18) [40,43].

With this strategy, when the exciton is formed near the interface the electron can be transferred to the second semiconductor, the hole can travel between the donor semiconductor and the negative electrode, and the electron between the accepting semiconductor and the positive electrode [40,43].

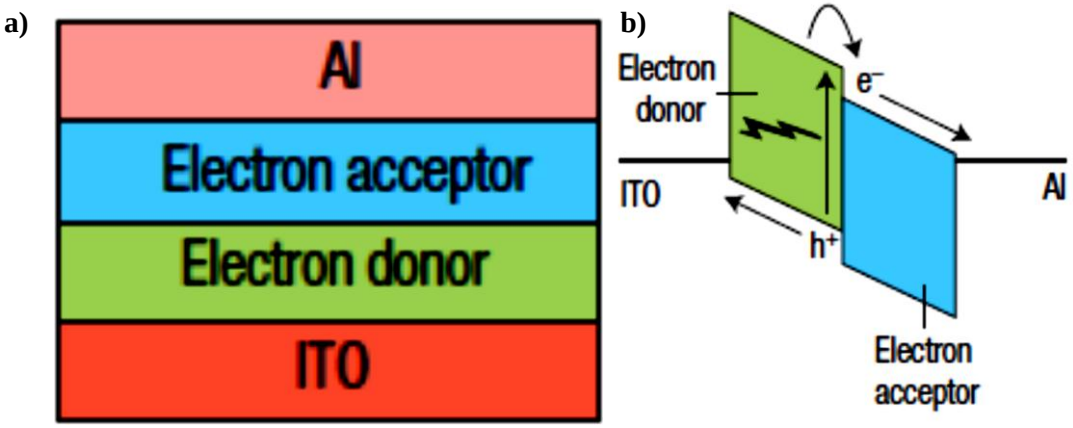

Figure I.18: Representation of a model a) and a schematic energy band b) of a bilayer-layer semiconductor – polymer solar cell [43].

Polymers need typically 100 nm to absorb enough light, but in these devices only excitons created within the distance of 10-20 nm from the interface can reach the heterojunction and consequently, losses of absorption and low quantum efficiencies are observed [40,43].

Trying to reduce this effect, the ITO electrode is structured by chemical etching using PEDOT:PSS (like is represented in Figure I.19), thus improving the surface quality of the ITO.

This strategy minimizes the photocurrent at the maximum of the optical absorption spectrum and improves the efficiency of the devices [40].

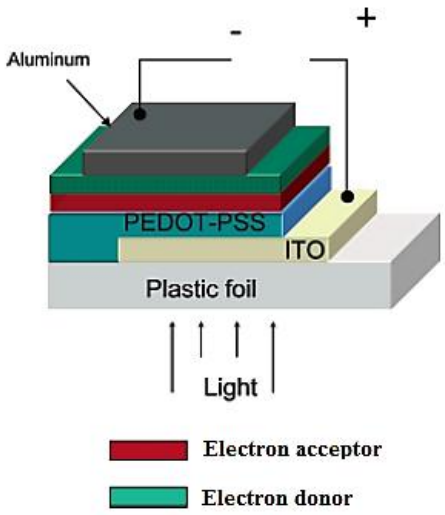

Figure I.19: Representation of a bilayer OPV device using a PEDOT:PSS layer [40].

Bulk Heterojunction Devices

Bulk heterojunctions are currently the most preferred architectures for OPV devices. While in the bilayer devices the semiconductors are completely separated from each other and can have selectively separate contact the electrodes, in this case phases are intermixed (see Figure I.20) [40,43].

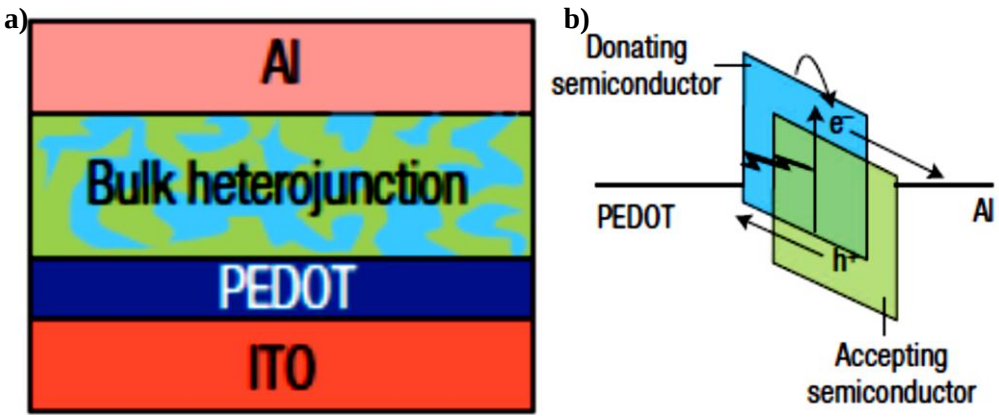

Figure I. 20: Representation of a model a) and a schematic energy band b) of a bulk heterojunction organic solar cell [43].

Usually the donor-acceptor phase separation occurs is a 10-20 nm length scale, which avoids the exciton phenomenon and improves the efficiency of OPV cells. Here, there is no preferential direction for the internal fields of separated charges and, because of this, the electrons and holes created inside do not have a defined movement direction, having as a driving force only the concentration gradient [40].

By using symmetry breaking conditions (*e.g.* different electrodes) the interpenetrating network formed by the semiconductors and the morphology are extremely important since they can completely change the performance of the device [40].

This type of architecture is reported to give the best results. Several systems have been tested with different polymers conjugations (*e.g.* MDMO-PPV/C_{60}, MDMO-PPV/PCBM, P3ATs/PCBM or PH3T/PCBM) and despite the results are promising, much work is still needed in this field [30,40].

Tandem cells (represented on Figure I.21) are a variant of bulk heterojunction devices. Build layer by layer, these devices have an intermediary layer between the different heterojunctions. This intermediate layers are inserted to improve the devices once they can reduce the losses and increase the efficiency [44]. Different groups such as Handipour *et al.* [45], Xue *et al.* [46] or Maenning *et al.* [47] have been studying different systems of tandem cells with some promising results that allowed an improvement of the efficiencies in some cases up to 6% [30,44].

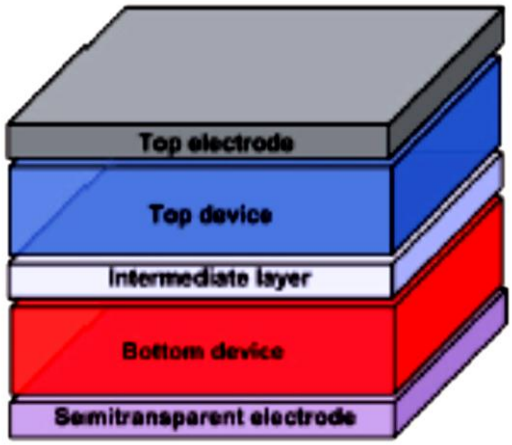

Figure I.21: Generic representation of a tandem organic solar cell [44].

iii. Hybrid solar Cells

The hybrid solar cells emerged as an alternative to low efficient OPV cells by combining the unique properties of inorganic semiconductors with the film-forming properties of organic semiconductors.

The production strategy for this type of solar cells is the use of blends of nanocrystals with semiconductive polymers as the bulk heterojunction devices, avoiding the problem of the exciton phenomenon. The only disadvantage of these devices is the solubility of the organic and the inorganic semiconducting nanoparticles, once the first is commonly soluble in organic solvents and the second in aqueous solvents. This is the reason why a ligand exchange is used in these cells, once it would turn the nanoparticles soluble in organic solvents [40,48].

This is a field still in development and the systems need to be improved to have a good cost-efficiency correlation, nevertheless these are very promising devices.

iv. Performance Characteristics

Before the introduction of the PV cell on the market is mandatory to study a number of different parameters to evaluate the performance of the PV cell.

The characteristic current-voltage curves of a PV cell, in the dark and under illumination, are shown on Figure I.21. In this curves, is possible to observe that in the dark, there is almost no current flowing, until the contacts start to inject at forward bias for voltages larger than the V_{oc}. Between (a) and (b) the device generates power under light and at MPP, the product of current and voltage is the largest [40].

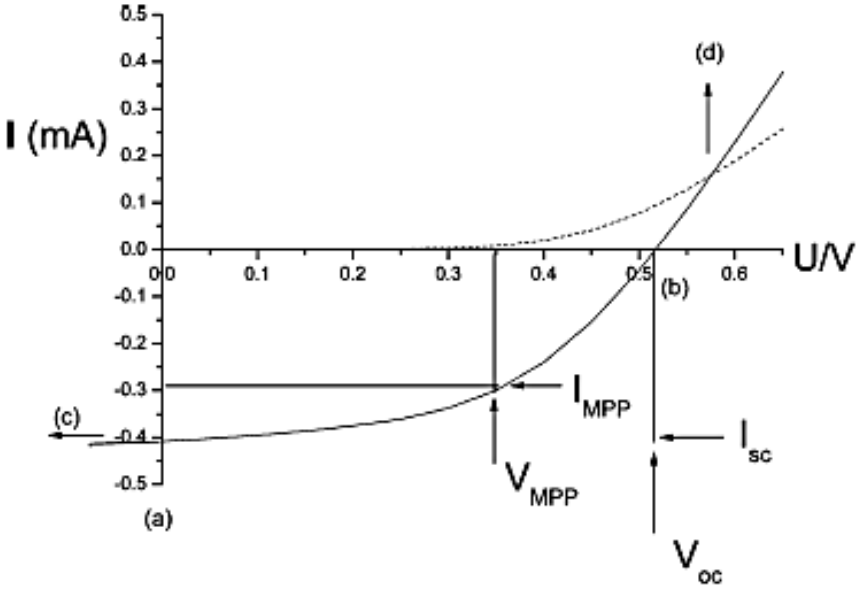

Figure I.22: Representative current-voltage (I-V) curves for an organic solar cell. The characteristic intersections with the abscissa and ordinate are V_{oc} and the I_{sc}, respectively. P_{max} is determined by the point where the product of voltage and current is maximized [40].

One of the most important parameters of a solar cell is a good PCE. Equation 1 defines the PCE:

$$\eta_e = \frac{I_{sc} \times V_{OC} \times FF}{P_{in}} \quad (1)$$

The P_{in} value is standardized at 1000 W/m^2 with a spectral intensity distribution identical to the sun on Earth's surface at an incident angle of 48.2^O. The V_{oc} of a metal-insulator-metal cell is 0 (see Figure I.22), corresponding to almost flat valence and conduction bands [39,40,48].

The I_{sc} is the maximum photocurrent density (the only which crosses the cell at zero applied voltage as it shown on figure I.22), which is determined by the product of photoinduced charge carrier density and the charge carrier mobility within the organic semiconductors, represented by Equation 2:

$$I_{sc} = ne\mu E \tag{2}$$

where *n* is the density of charge carriers, *e* is the elementary charge, μ is the mobility and *E* is the electric field .

The FF is the ratio of the maximum power to the external I_{sc} and V_{oc} as shown in Equation 3:

$$FF = \frac{P_{max}}{I_{sc} \times V_{OC}} \tag{3}$$

IPCE is the external quantum efficiency and is also other important parameter, calculated using Equation 5:

$$IPCE = \frac{1240\ I_{sc}}{\lambda P_{in}} \tag{5}$$

This represents the number of electrons collected under I_{sc} ($\mu A/cm^2$) conditions divided by the number of incident photons, calculated by the product of the incident photon wavelength (nm) and the incident power (W/m^2) [40].

f. Artificial Leaves

Recently, the investigation of OPV cells has been focused on biomimetic or biocompatible solar cells, based on "artificial leaves". This new class of OPV uses photoactive biocomplexes (*e.g.* chlorophyll) as photosensitizers of the biomimetic solar cells prototypes [49]. Lai *et al* [50], Terasaki *et al.*[51], Ciesielski *et al.*[52] and Murakami *et al.*[53] have been active in this area [49]. Artificial leaves use chemical or physical linkers to allow the transference of electrons between photoelectrodes, biocompatible solvents and materials, such as water, lipid membranes or agarose. Systems based on ionic photovoltaics and hydrogels has been also investigated as sustainable alternatives [49].

g. Novel Artificial Leaves

The main objective of this thesis was the development of a novel flexible hydrogel-based, low cost and biocompatible "artificial leaf". From previous work [54,55] is known that to reach high efficiencies, the photoactive species (donor-acceptor) must be closer enough to enable excited state charge transfer. Therefore, a novel solution was proposed in order to create

a system where the photoactive species were embedded in a gel matrix with a nanosized phase separation. In the chosen system, the organic semiconductor is a dendrimer, once the 3D structure of this type of polymers allow a perfect location of active sites, and enable highly efficient electron-transfer processes [39,56].

Moreover, this type of polymers can be synthesized using a green $scCO_2$-assisted technology as it was described before by Restani *et al.* [20], and being a solvent for monomers and a non-solvent for polymers, CO_2 allows their easy separation at the end of the reaction by simple depressurization. Other important advantage of this technology is that CO_2 can also act as a reagent (C1 feedstock) and be incorporated in the dendrimers backbone. In this thesis the first step of the "artificial leaf" construction is the synthesis of a PURAM-type dendrimer, where TAPA is used as a key building block (Figure I.23).

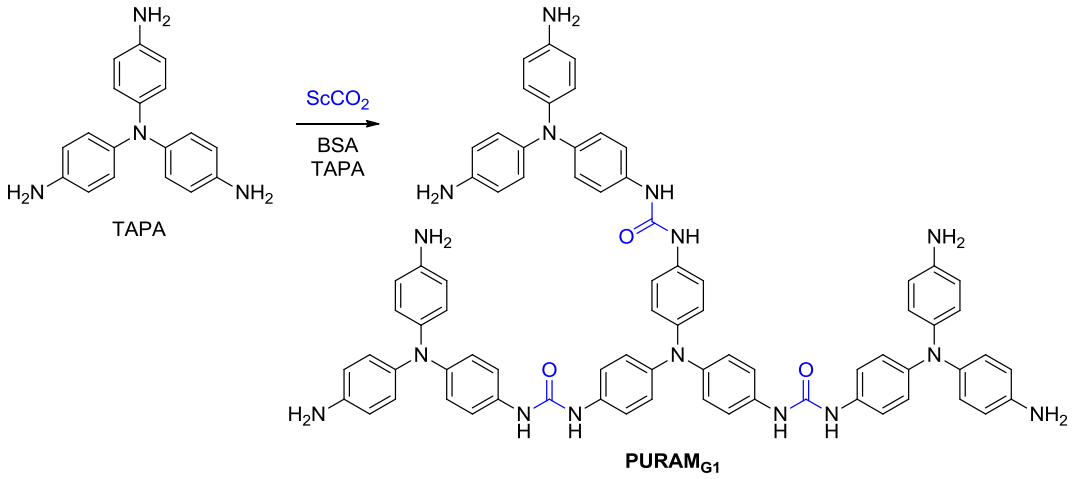

Figure I.23: Schematic synthesis of the $PURAM_{G1}$ dendrimer in $scCO_2$.

The formation of urea linkages (by incorporation of CO_2 in the dendrimers backbone) is crucial since they will be essential for further construction of the 1,3-diphenyl-imidazoline-2-one scaffold, the acceptor unit (Figure I.24). Conjugated with arylamines (donor species) and other aromatic scaffolds, the imidazolinone moiety is reported to have excellent charge transporting properties, heat resistance, amorphous nature, solubility and redox stability, important characteristics for OPV devices [57]. The incorporation of imidazolones into our "artificial leaf" is easily achieved by reacting the $PURAM_{G1}$ dendrimer with benzoins under heating. The obtained PIMAM-type dendrimers are composed of conjugated donor and acceptor species (Figure I.24) [58].

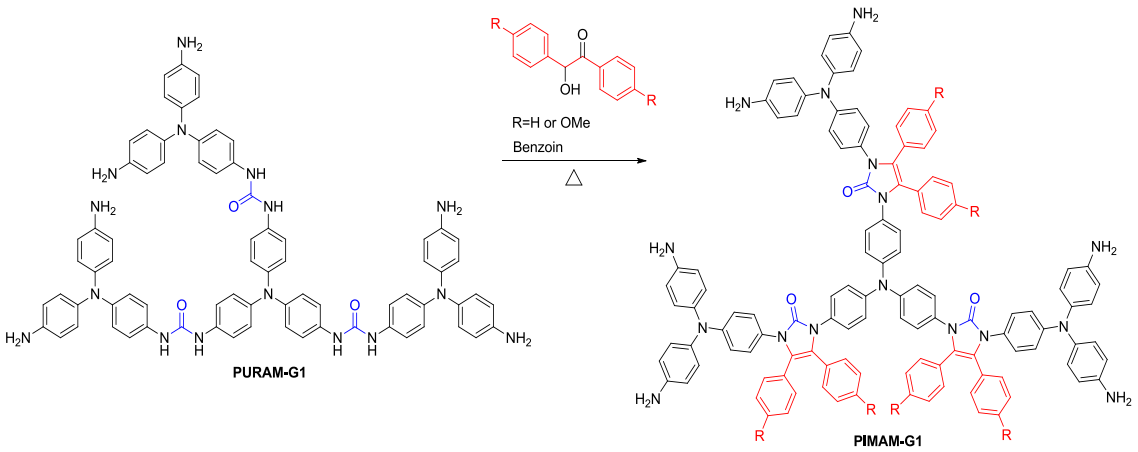

Figure I.24: Schematic synthesis of $PIMAM_{G1}$ dendrimers.

One of the main goals of this thesis is the development of water-soluble OPVs. Since $PIMAM_{G1}$ has a low solubility in water, further surface functionalization is required. Therefore, reaction with hydrophilic amines, like TREN or Sigma 7-9, will allow tuning the dendrimers solubility in water.

Having the OPV component synthesized, the next step is the assembly of the dendrimer unit with a sensitizer to obtain the desired host-guest photoactive species in the polyelectrolyte (hydrogel) transporting medium. In the proposed strategy the dendrimers, possessing a pendant cavity, will act as nanovelcros, being able to accept the sensitizer in their cavity. $[Ru(bpy)_3]^{2+}$ is one of the most studied systems for dye-sensitized photovoltaic cells, since is chemical stable, presents a long-lived excited state at room temperature and holds good luminescent properties [59]. For these reasons $[Ru(bpy)_3]^{2+}$ was elected as the sensitizer, and was functionalized with ferrocene units (Figure I.25), thus allowing its incorporation in the dendrimers pendant cavities.

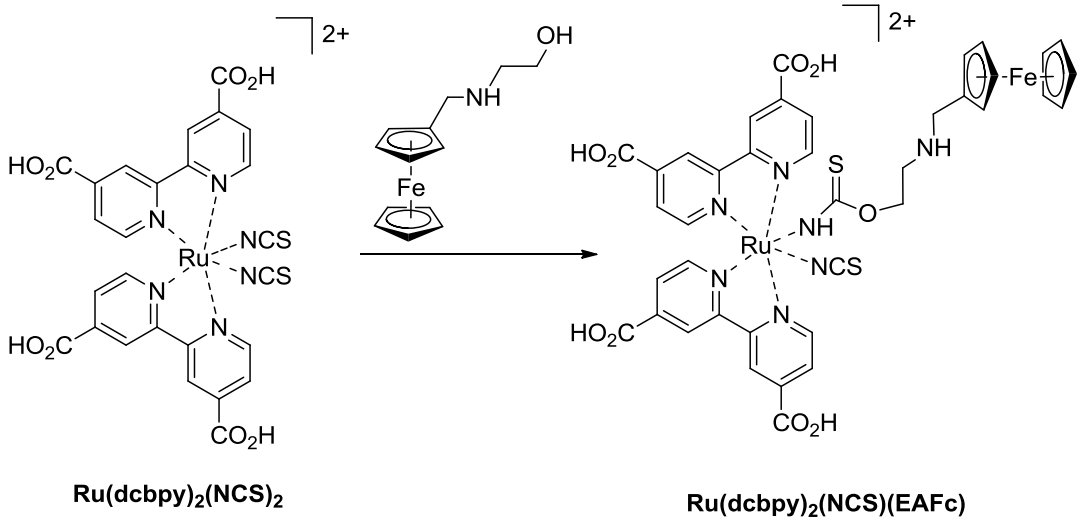

Figure I.25: Synthesis of a Ru(II) dye sensitizer functionalized with a ferrocene unit.

Recently, a supramolecular velcro has been developed for a reversible underwater adhesion of chip surfaces [60] using modified curcubit[7]uril ([CB]7) cavity. This macrocycle is able to establish very strong inclusion complexes with ferrocene derivatives [60,61]. However, CB[7] is a highly expensive macromolecule and its modification, in order to be used as a nanovelcro $(allyloxy)_1CB[7]$), is made in two steps having a very low yield (*ca.* 4%). In this sense, β-CD is a good alternative since has approximately the same cavity size of CB[7] (Figure I.26), is able to establish good inclusion complexes with ferrocenes (although not so strong like CB[7]), and has interesting electrochemical properties [61-63]. Moreover, the synthesis of clickable per-6-thio-β-cyclodextrin, starting from β-CD, is reported to be achieved in two high yielding steps [64,65].

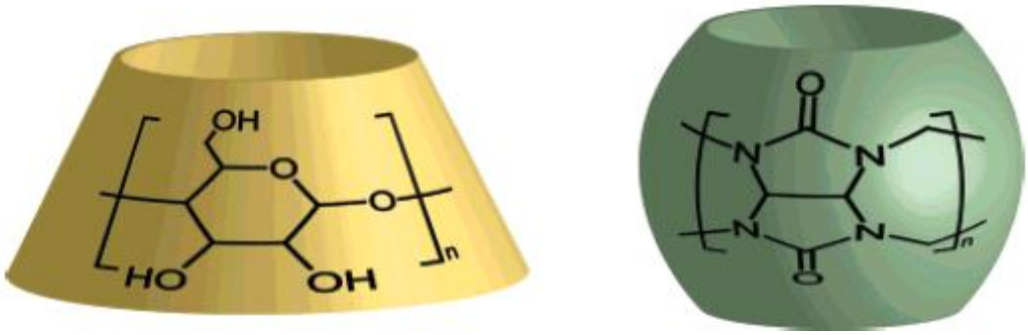

Figure I.26: Schematic comparison between cyclodextrins (left) and curcubiturils (right) structures [61].

Finally, the allylation of dendrimer unit will allow the conjugation of the per-6-thio-β–cyclodextrin (via a thiol-ene click reaction) and further complexation with the Ruthenium (II) sensitizer and preparation of the hydrogel-based solar cell device.

II. Materials and Methods

i. Materials

Carbon dioxide was obtained from Air Liquide with purity higher than 99.998%. All chemicals and solvents were used as received without further purification. TAPA (97% purity), DMF anhydrous (99.8% purity), NaH, (57-68% purity), BSA (95% purity), allyl bromide (99% purity), iodine (>99% purity) and TREN (97% purity) were purchased from Alpha Aesar. Benzoin (> 98.0% purity) was purchased from TCI and 4,4'-dimethoxybenzoin from MP. PPh_3 (≥ 98.5% purity) and CH_3ONa (≥ 95% purity) were acquired from Fluka, Ethanolamine (>99% purity) from BDH, Thiourea (pro analisys, min. 99.5% purity) from Merck, Sigma 7-9 (≥ 99% purity) and β-CD (minimum 98% purity) from Sigma. $Ru(dcbpy)_2(NCS)_2$ (95% purity), $NaBH_4$ (98% purity) and tetrabutylammonium tetrafluoroborate (for electrochemical analysis, ≥ 99.0%) were purchased from Sigma-Aldrich.

ii. Methods

UV-Vis spectra were obtained in a *UV-1700 PharmaSpec Spectrometer* from Shimadzu over the spectral range of 200 to 900 nm with a scan rate of 100 nm min^{-1} at 25 °C in 1 cm cuvettes.

The fluorescence spectra were recorded at 25 °C on a *PerkinElmer LS 45 Luminescence Spectrometer* with a slit with of 5 nm at a scan rate of 240 nm min^{-1}.

The NMR spectra were recorded on a *Bruker ARX 400 MHz* equipment. ^{1}H and ^{13}C NMR chemical shifts are reported as ppm (ppm= parts per million). The NMR spectrometer is part of the National NMR Network (RNRMN) and is funded by "Fundação para a Ciência e Tecnologia" (FC&T).

Dried samples were analyzed on a Fourier Transform Infrared (FTIR) in a *Spectrum BX* from *PerkinElmer* and the spectrum acquisition was made by 16 scans, at a range of 4000 to 600 cm^{-1}.

iii. Experimental Procedures

Synthesis of $PURAM_{G1}$ dendrimer and derivatives

The PURAM dendrimers synthesis followed a reported protocol [20]. Typically, the synthesis was performed in a 33 mL stainless-steel high-pressure cell that was loaded with 0.500 g of TAPA (1.72 mmol), 1.69 mL of BSA (6.88 mmol) and 1 mL of DMF anhydrous (to help the solubilization) under stirring conditions. The reactor was then closed with two aligned sapphire windows, connected to the CO_2 line charged with gas to approximately 0.1 MPa and placed in a thermostated water bath at 40 ^{O}C to assure control and avoid gas leakage from the

reactor. After that, the pressure was finally adjusted to 18.5 MPa by addition of further CO_2 to solubilize the substrates.

The reaction was allowed to proceed under a homogenous supercritical phase for 20 h before washing during 1 h and depressurization. In second step of the reaction, the cell was opened in order to add more TAPA (1.52 g, 52.5 mmol) and BSA (2.95 mL, 12.0 mmol). The mixture was kept at 120 ^{O}C for 17 h under stirring.

After that acetone was added into the cell and the crude was removed and filtrated at vacuum obtaining a dark purple solid (2.00 g) with 93.6% yield.

Due to its low solubility in most of organic solvents, including DMSO and $CHCl_3$, was not possible to fully characterize the $PURAM_{G1}$ dendrimer. The ^{1}H-NMR shows a broad signal between 6.8 and 7 ppm.

FTIR (KBr) υ (cm^{-1}): 3379 (Ar-NH_2), 1697 (C=O from urea), 1635, 1625, 1594 (N-H from urea), 1504 (Ar-H), 1315 (Ar-H), 1271 (Figure VI.1, Appendix I).

$PURAM_{G1}$ derivatives, PUPA dendrimers, were synthesized using the same protocol, but in the second step TREN (0.790 mL, 5.25 mmol) was added instead of TAPA. In the end of the reaction a highly insoluble gray solid was obtained, thus precluding further characterization.

PURAP dendrimers were also synthesised. Following the usual protocol, in first step TREN (0.100 mL, 0.680 mmol) and BSA (0.670 mL, 2.74 mmol) were added to the cell, followed by TAPA (0.606 g, 2.09 mmol) and more BSA (1.18 mL, 4.79 mmol) and in second step. The crude product was removed from the cell by addition of acetone and filtrated under vacuum. A purple solid was obtained. The filtrate was dried under vacuum, and gave a purple oil (0.346 g) with 46.4% yield.

FTIR (NaCl film) υ (cm^{-1}): 3390 (Ar-H), 1654 (C=O from urea), 1399 (CH_2) (Figure VI.2, Appendix I)

^{1}H NMR (400 MHz, DMSO-*d6*) δ (ppm): 7.43–7.05 (m, 4H), 7.04–6.32 (m, 12H), 3.44 (s, 4H) (Figure VI.3, Appendix I).

^{13}C NMR (101 MHz, DMSO-*d6*) δ (ppm): 171.46, 143.16, 138.63, 124.05, 114.79, 114.72, 22.48 (Figure VI.4, Appendix I).

Synthesis of $PIMAM_{G1}$ derivatives

Two PIMAM dendrimers using different benzoins, namely benzoin ($PIMAM_{G1}$) and 4,4'-dimethoxybenzoin (PIMAM-OMe_{G1}) were synthesized. The synthesis followed a modified protocol [58].

In a 50 mL round bottom flask, benzoin (0.385 g, 1.81 mmol) or 4,4'-dimethoxybenzoin (0.494 g, 1.81 mmol) was added to $PURAM_{G1}$ (0.500 g, 0.400 mmol) and the mixture was

heated using an oil bath (170 ^{O}C) under stirring during 17 hours. The mixture was then washed with acetone and a black solid was collected by filtration under vacuum.

$PIMAM_{G1}$:

Yield: 60.0% (0.435 g). FTIR (KBr) υ (cm^{-1}): 3446 (Ar-NH_2), 1636 (C=O imidazolone ring), 1507 (Ar-H), 1309 (Ar-H), 1273 (Ar-H), 832, 618 (Figure VI.5, Appendix II).

^{1}H NMR (400 MHz, DMSO-*d6*) δ (ppm): 7.93 (t, *J*= 6.7 Hz, 12H, H_c), 7.84–7.77 (m, 6H, H_a), 7.71–7.56 (m, 24H, H_b and H_d), 7.55–7.30 (m, 36H, H_e) (Figure VI.6, Appendix II). Due to low solubility in DMSO-*d6* it was not possible to obtain a ^{13}C NMR spectrum with enough resolution.

$PIMAM\text{-}OMe_{G1}$:

Yield: 40.0% (0.318 g). FTIR (KBr) υ (cm^{-1}): 3421 (Ar-NH_2), 1619 (C=O imidazolone ring), 1508 (Ar-H), 1312 (Ar-H), 1260 (Ar-H), 1175 (C-O-C) (Figure VI.7, Appendix II).

^{1}H NMR (400 MHz, DMSO-*d6*) δ (ppm): 7.73 (t, 12H, H_b), 7.00-6.98 (d, 12H, H_c), 6.98-6.66 (broad signal, 54H, H_e and H_d), 3.81(s, 18 H, H_a) with a little contamination of 4,4'-dimethoxibenzil (secondary product formed, as result of oxidation of 4,4'-dimethoxibenzoin) at 7.83 (d, 4H), 7.12 (d, 4H) and 3.81 (s, 6H). (Figure VI.8, Appendix II). Due to low solubility in DMSO-*d6* it was not possible to obtain a ^{13}C NMR spectrum with enough resolution.

Synthesis of $PIMAM_{G2}$

$PIMAM_{G2}$ dendrimers synthesis is the same way of $PURAM_{G1}$ (following the procedure described in ref. [20]), only changing the monomers. In first step was added into the cell 0.402 g (0.227 mmol) of $PIMAM_{G1}$, 0.391 mL of BSA (1.59 mmol) and 1 mL of DMF anhydrous. In second step of the reaction, was added into the cell 0.196 mL (1.38 mmol) of TREN and more BSA (0.725 mL, 2.96 mmol).

In the end of the reaction, the cell was opened and the crude was removed by addition of water into the cell and water purified by dialysis (using a dialysis Cassettes G2 with a 2000 MWCO purchased at Thermo Scientific) and dried under vacuum.

After this purification the compound became insoluble in water and order organic solvents and the characterization by NMR, once the only thing that is visible is the TREN who did not react.

FTIR (KBr) υ (cm^{-1}): 3421 (Ar-NH_2),3023, 1640 (C=O imidazolone ring), 1215 (Ar-H) (Figure VI.9, Appendix III).

A derivative of $PIMAM_{G2}$, $PIMAM\text{-}OH_{G2}$, was also synthesized. Following the same procedure of $PURAM_{G1}$ synthesis, in first step was added into the cell 0.250 g (0.128 mmol) of

PIMAM-OMe_{G1}, 0.220 mL (0.898 mmol) of BSA and 1 mL of DMF anhydrous. In second step of the reaction, was added into the cell 0.0940 g (0.776 mmol) of Sigma 7-9 and more BSA (0.409 mL, 1.67 mmol).

The crude was washed with water and after that was removed from the cell by addition of methanol the solution was dried under vacuum giving a black solid (0.216 g) with a yield of 59.7%.

FTIR (KBr) υ (cm^{-1}): 3343(Ar-NH_2 and OH), 2938 (C-CH_2), 2847 (C-CH_2), 1654 (C=O), 1633 (C=C), 1594 (Ar-H), 1507 (Ar-H), 1040, 1023 (Figure VI.10, Appendix III).

^{1}H NMR (400 MHz, DMSO-*d6*) δ (ppm): 7.36-6.51 (m), 4.40 (s,), 3.75-3.26 (m). ^{13}C NMR (101 MHz, DMSO-*d6*) δ (ppm): 171.91, 63.60, 61.83, 61.74, 61.29, 57.48, 22.97.

Allylation of PIMAM-OH_{G2} and PIMAM-OMe_{G1}

Following a modified protocol [60] in 50 mL round bottom flask, under nitrogen atmosphere, was added 0.0281g (0.546 mmol) of NaH to a stirred solution of 0.150 g (0.0530 mmol) of PIMAM-OH_{G2} in 3 mL of DMF anhydrous cooled to 0 ^{O}C . The mixture was warmed to room temperature and stirred during 30 minutes. After that, 0.0500 mL (0.546 mmol) of allyl bromide was added dropwise and the mixture was kept stirring under nitrogen conditions during 17 hours.

The NaH who did not react was destroyed by the addition of ice into the mixture, at 0 ^{O}C. The solid precipitated was filtered under vacuum and washed with chloroform, giving a black solid (allyl-PIMAM-OH_{G2}, 0.0294g)

FTIR (KBr) υ (cm^{-1}): 3445 (OH), 2917 (C-CH_2), 1638 (C=O), 1508 (Ar-H), 1025 (C-OH), 617 (C-Br, a contamination from allyl bromide) (Figure VI.11, Appendix IV).

After purification, it was not possible to obtain neither ^{1}H NMR or ^{13}C NMR spectra, due of the insolubility of this compound.

PIMAM-OMe_{G1} was also allylated using the same procedure followed for PIMAM-OH_{G2}, using 0.0780g (1.38 mmol) of NaH, 0.490 g (0.251 mmol) PIMAM-OMe_{G1}, 5 mL of anhydrous DMF and 0.16 mL of allyl bromide giving a black solid (allyl-PIMAM-OMe_{G1}, 0.483 g) with 16.0% yield.

FTIR (KBr) υ (cm^{-1}): 3432 (OH), 2924 (C-CH_2), 2848 (C-CH_2), 1658 (C=O), 1602, 1510 (Ar-H), 13113, 125 (Figure VI. 12, Appendix IV).

^{1}H NMR (400 MHz, DMSO-*d6*) δ (ppm): 7.95-6.74 (m, 24H, H_a), 5.76 (s, 2H,H_c), 5.09 (s, 4H, H_d), 4.49-3.97 (m, 4H, H_b), 3.88-3.60 (m, 7H, H_e) (Figure VI.13, Appendix IV).

Due to the low solubility in DMSO-*d6* it was not possible to obtain a ^{13}C-NMR spectrum with enough resolution.

Reductive Amination of Ferrocenecarboxaldehyde

Based on procedure described in ref. [65]. In a 50 mL round-bottom flask, Fc (0.4922g, 2.34 mmol) was added to a stirred solution of 40% aqueous ethanolamine (7.2 mL in 18 mL of water) at 0 ºC. The solution was allowed to warm to room temperature and stirred for 2 days. The reaction mixture was washed with water and the orange solid was dried under vacuum.

Reduction with $NaBH_4$

In a 50 mL round-bottom flask, the previous compound was added to a suspension of $NaBH_4$ (0.249 g, 6.53 mmol) in 31 mL of ethanol. The solution immediately turned yellow-orange and was allowed to stir for 2 h at room temperature under nitrogen atmosphere.

The volatiles were removed in vacuum and the product was extracted with ethyl ether. The combined ether extracts were washed with water and dried over $MgSO_4$. The volatiles were removed in vacuum to give EAFc as a yellow-orange solid (0.284 g) with a yield of 46.6 %.

FTIR (KBr) υ (cm^{-1}): 3423 (OH), 3082 (Ar-H), 2900 (C-CH_2), 2832 (C-CH_2), 1634 (NH), 1429 (C-CH_2), 1062 (C-OH) (Figure VI.14, Appendix V).

^{1}H NMR (400 MHz, $CDCl_3$) δ (ppm): 4.27-4.15 (m, 4H, H_a and H_b), 4.13 (s, 5H, H_c), 3.64 (s, 2H, H_f), 3.55 (s, 2H, H_d), 2.78 (s, 2H, H_e) (Figure VI.15, Appendix V).

^{13}C NMR (101 MHz, $CDCl_3$) δ (ppm): 69.16-68.00 (C_a, C_b and C_c), 60.54 (C_f), 50.51 (C_e), 48.42 (C_d) (Figure VI.16, Appendix V).

Synthesis of the ruthenium derivative $Ru(dcbpy)_2(NCS)(EAFc)$

Following the procedure described in ref. [66], in a 50 mL round-bottom flask, 0.0949 g (0.0841 mmol) of $Ru(dcbpy)_2((NCS)_2$ was added to a stirred solution of 0.111 g (0.421 mmol) of EAFc and 0.0172 g (0.421 mmol) of NaOH in 2.8 mL of water and poured into an oil bath at 50 ^{O}C during 2 hours.

The mixture was cooled to room temperature and was added 14 mL of water and the pH was adjusted to 1, precipitating a solid that was collected by filtration under vacuum, obtaining the $Ru(dcbpy)_2(NCS)$(EaFc), a purple solid (0.0424g) with a yield of 38.1%.

FTIR (KBr) υ (cm^{-1}): 3416 (OH), 3074 (Ar-H), 2101 (C=S), 1705 (Ar-H), 1609 (Ar-H), 1258 (C-CH_2), 1230 (C-CH_2) (Figure VI.17, Appendix VI).

^{1}H NMR (400 MHz, DMSO-*d6*) δ (ppm): 9.49-9.26 (m, 2H, H_a), 9.06 (d, *J*= 69.2 Hz, 4H, H_c), 8.32 (d, *J*= 4.9 Hz, 2H, H_a), 7.66 (dd, *J*= 71.6, 21.7 Hz, 4H, H_c), 4.69-3.76 (m, 18H, H_g), 3.63 (s, 2H, H_d), 3.15 (s, 4H, H_f), 2.94 (d, *J* = 27.4 Hz, 1H, H_e), 1.55 (s, 4H), 1.29 (d, *J*= 6.5 Hz, 4H), 0.91 (t, *J* = 6.8 Hz, 6H) (Figure VI.18, Appendix VI).

^{13}C NMR (101 MHz, DMSO-*d6*) δ (ppm): 165.73, 165.16, 158.55, 157.12, 139.79, 134.35, 125.39, 74.09, 69.52, 67.85, 64.41, 23.06, 19.18 (Figure VI.19, Appendix VI).

Synthesis of Per-6-iodo-β-cyclodextrin

Following the protocol from ref. [64], to a stirred solution of PPH_3 (2.460 g, 9.37 mmol) and iodine (2.37507 g, 9.37 mmol) in DMF (9.5 mL) was added 0.505 g of β-CD (0.445 mmol) and the solution was stirred at 80 °C for 15 h. The pH was adjusted to 9-10, by the addition of sodium methoxide in methanol (3M), with simultaneous cooling. The solution was kept at room temperature for 30 min, after which it was added ice water precipitating a brown solid that was collected by filtration and this solid was washed with acetone giving a white solid (0.365 g) representing a yield of 48.7%.

FTIR (KBr) υ (cm^{-1}): 3362 (OH), 1152, 1064, 1037 (Figure VI.20, Appendix VII).

^{1}H NMR (400 MHz, DMSO-*d6*) δ (ppm): 6.03 (d, *J*= 6.8 Hz, 7H,OH_b), 5.92 (s, 7H, OH_c), 4.99 (s, 7H, H_a), 3.81 (d, *J*= 9.7 Hz, 7H, H_b), 3.71-3.55 (m, 14H, H_c and H_e), 3.53-3.35 (m, 21H, H_d and H_f) (Figure VI.21, Appendix VII).

^{13}C NMR (101 MHz, DMSO-*d6*) δ(ppm): 102.60 (C_a), 86.41 (C_d), 72.64, 72.38 and 71.41 (C_c and C_e), 31.17 (C_b), 9.94 (C_f) (Figure VI.22, Appendix VII).

Synthesis of Per-6-thio-β-cyclodextrin

As it described in ref. [65], 0.510g (0.000263 mol) of per-6-iodo-β-cyclodextrin was dissolved in anhydrous DMF (5.5 mL). Then 0.160 g thiourea (0.0021 mol) was added and the reaction mixture heated to 70 ^{O}C under a nitrogen atmosphere. After 19 h, the DMF was removed under reduced pressure to give a yellow oil, which was dissolved in water (27 mL). Sodium hydroxide (0.144 g) was added and the reaction mixture heated to a gentle reflux under a nitrogen atmosphere. After 1 h, the resulting suspension was acidified until pH 3-4 with aqueous $NaHSO_4$ and the precipitate filtered off, washed thoroughly with distilled water, and dried. The product was suspended in water (27 mL) and the minimum amount of potassium hydroxide added to give a clear solution; the product was then re-precipitated by acidifying with aqueous $NaHSO_4$.The resulting fine precipitate was carefully filtered off and dried under vacuum over, obtaining a white solid (0,0981 g) with a yield of 33.4%.

FTIR (KBr) υ (cm^{-1}): 3604 (OH), 2926 (C-CH_2), 2561 (S-H), 1638, 1406, 1154, 1043 (C-O-C) (Figure VI.23, Appendix VIII).

^{1}H NMR (400 MHz, DMSO-*d6*) δ (ppm): 5.88 (dd, *J*= 31.7, 13.4 Hz, 14H, OH_b, OH_c), 4.91 (d, *J*= 16.2 Hz, 7H, H_a), 3.72-3.51 (m, 22H, H_e, H_c), 3.24-3.14 (m, 44H, H_b, H_d, H_f), 2.84-2.68 (m, 7H, H_f), 2.19-2.06 (m, 6H, SH) (Figure VI.24, Appendix VIII).

^{13}C NMR (101 MHz, DMSO-*d6*) δ (ppm): 102.18 (C_a), 84.91 (C_d), 72.29 (C_b, C_c, C_e), 25.95 (C_f) (Figure VI. 25, Appendix VIII).

Fluorescence Studies

The fluorescence of PIMAM-OMe_{G1} and $Ru(dcbpy)_2(EAFc)_2$ solutions (in DMSO) were measured exciting the molecules at λ_{max}, respectively, 311 nm for PIMAMOMe_{G1} and 318 nm, 402 nm and 541 nm for $Ru(dcbpy)_2(NCS)(EAFc)$ (Abs= 0.1).

Electrochemical properties of PIMAM-OMe_{G1} and $Ru(dcbpy)_2(NCS)(EAFc)$

The HOMO and LUMO energy levels of PIMAM-OMe_{G1} were estimated by CV using a three electrode scheme. The measurements were performed at 50 mV/s in an electrolyte solution of 0.1 M tetrabutylammonium tetrafluoroborate in acetonitrile (HPLC grade). The working electrode was a platinum disc, the reference electrode was a saturated calomel electrode (SCE), and the counter electrode was a platinum wire. HOMO and LUMO levels were estimated as corresponding to the onset potentials for oxidation and reduction, respectively, after referencing the measured potentials to the vacuum level (for this, we used Fc/Fc+ redox couple as external reference). The electrochemical properties of $Ru(dcbpy)_2(NCS)(EAFc)$ were measured as the same procedure.

III. Results and Discussion

Scheme III.1 shows the global synthetic plan realized for this thesis. As can be seen not all photoactive dendrimers were successful synthesized and/or characterized, mainly due to low solubility in common organic solvents and/or water. Because of that several strategies were explored to overcome this issue, namely, using different monomers in the second generation, like TREN or Sigma 7-9 but, unfortunately, without much success. We believe that the aromatic nature of the arylamine monomers (*e.g.* TAPA) is responsible for the observed aggregation leading to insoluble polymers, thus precluding (in some cases) a full characterization. The strategy adopted to enhance the solubility was the synthesis of PURAP dendrimers, which were found to be more soluble. It also was observed, that using 4,4'-dimethoxybenzoin, the solubility of the dendrimers slightly increases due to the presence of methoxy groups. For these reason this system was selected for further studies namely allyl-PIMAM-OH_{G2} and allyl-PIMAM-OMe_{G1} dendrimers.

In the reductive amination of Fc aldehyde was necessary to adopt a new strategy and change the amine, since the initial idea was use a diamine, but it was described on literature that this type of compounds are prone to dimerization [67]. That is the reason why we used ethanolamine, since the alcohol does not react with Fc aldehyde.

The use of β-CD appeared to be an excellent alternative to CB[7]. Our tries to modify CB[7] and incorporate it in our system were unsuccessful, the obtained yields were lower than described on literature (*ca*. 4%) [60]. Also the price of CB[7] is very high, thus lowering the economic potential of the solar cell devices. The found solution was to use β-CD, a natural macrocycle, as a less expensive starting material, that is reported to possess the same cavity size of CB[7] and the capacity of establishing inclusion complexes with ferrocene derivatives, although the binding constants of CB[7] inclusion complexes be 10^{9}-10^{13} M^{-1} and the binding constants of stable inclusion complexes with β-CD be on range of 10^{3}-10^{4} M^{-1} it is enough to make a stable inclusion complex has it was described before [61,68].

Fluorescence studies were performed for PIMAM-OMe_{G1} and $Ru(dcbpy)_2(NCS)(EAFc)$ in a preliminary study, to ensure that the compounds could absorb and emit light efficiently. These results (Figure III.1) shows that the $Ru(dcbpy)_2(NCS)(EAFc)$ does not have fluorescence, and that PIMAM-OMe_{G1} could emit energy on region where the sensitizer absorbs, which is a promising result. PIMAM-OMe_{G1} is the compound where we already have incorporated the photoactive specie with the donor and acceptor specie, the fundamental part of the system. If this specie already has this capacity the derivatives are also good choices for our system.

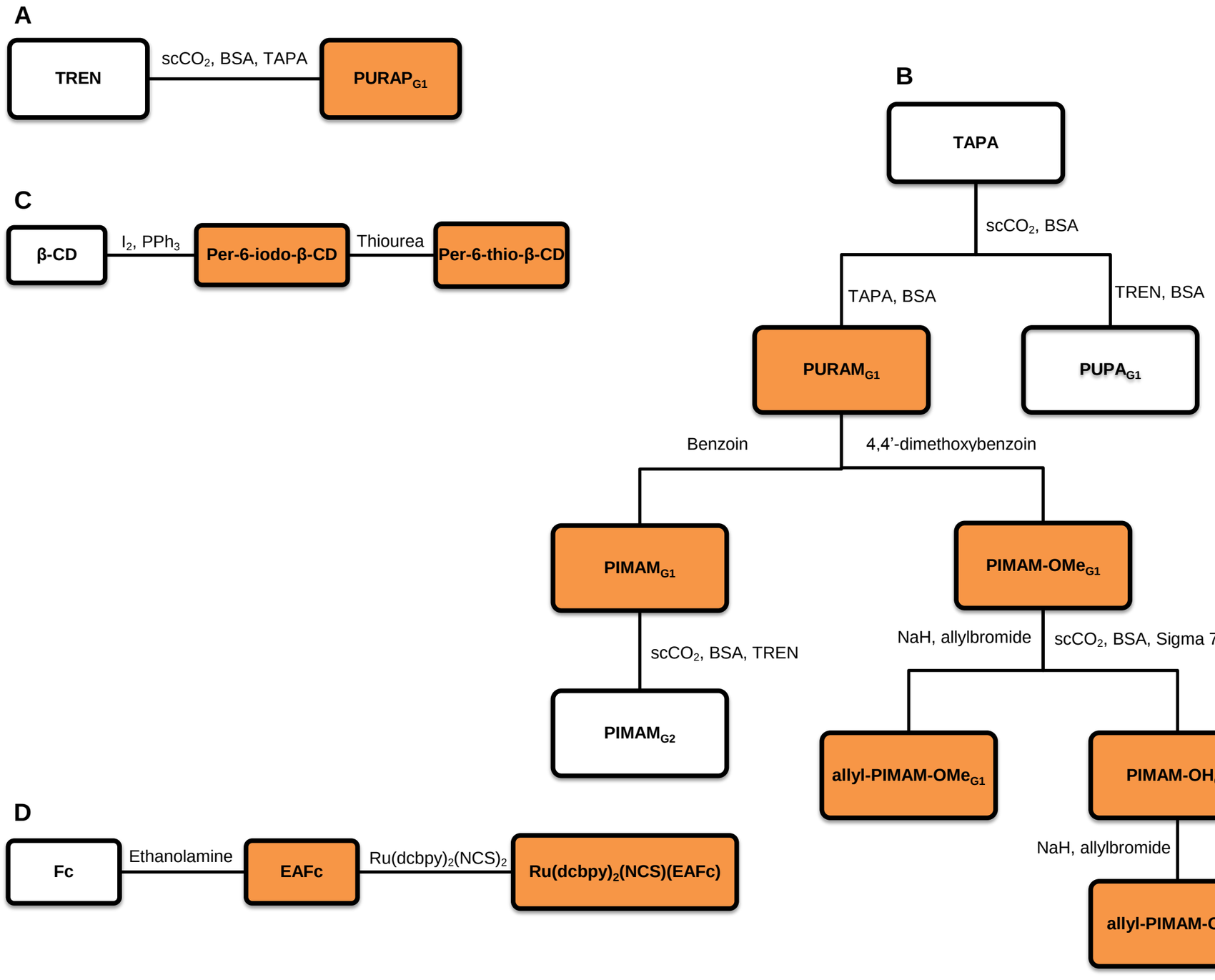

Scheme III.1: General synthetic route: A) synthesis of photoactive dendrimers using TREN as core; B) synthesis of photoactive dendrimers using TAPA as core; C) synthesis of β-CD derivatives; D) synthesis of the ruthenium (II) sensitizer. Orange boxes indicate a successful synthesis.

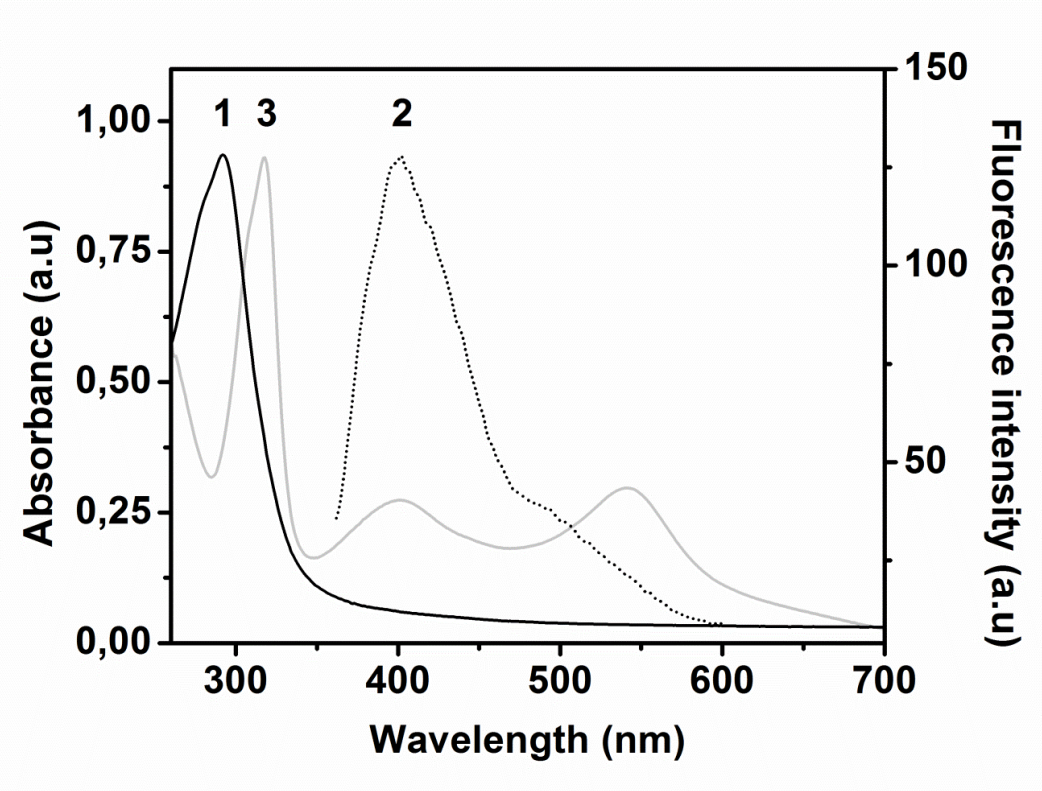

Figure III.1: Spectrocopic data for the solar cell components in DMSO: (1) absorbance spectrum of PIMAM-OMe_{G1} dendrimer, (2) emission spectrum of PIMAM-OMe_{G1} dendrimer, and (3) absorbance spectrum of $Ru(dcbpy)_2(NCS)(EAFc)$ sensitizer.

A preliminary CV study for these compounds was also performed. Therefore, it was possible to estimate the HOMO and LUMO levels as corresponding to the onset potentials for oxidation and reduction (Figure III.2), respectively, after referencing the measured potentials to the vacuum level (for this, we used Fc/Fc+ redox couple as external reference) [69]. As we measured $E_{1/2}$ (Fc/Fc^+)= 0.42 eV and the energy level of Fc/Fc^+ is at 4.80 eV below the vacuum level, we calculate:

HOMO (eV)= - ($E_{onset,ox}$ + 4.38) eV

LUMO (eV)= - ($E_{red,red}$ + 4.38) eV

Table III.1: Experimental values of onset potentials for oxidation and reduction and HOMO and LUMO energy levels estimated from CV data.

	$E_{onset,ox}$ (V)	$E_{red,ox}$ (V)	HOMO (eV)	LUMO (eV)
PIMAM-OMe_{G1}	**+1.58**	**-1.67**	**-5.96**	**-2.71**

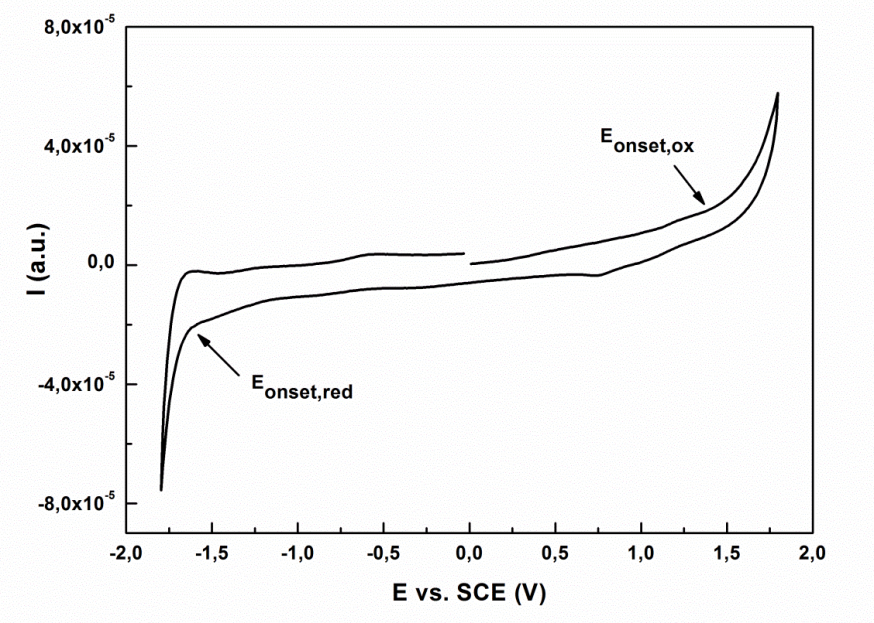

Figure III.2: Potential redox of the PIMAM-OMe_{G1} dendrimer.

The half-wave potentials for the three oxidation peaks of $Ru(dcbpy)_2(NCS)(EAFc)$ (Figure III.3), vs. SCE electrode observed in the 0-1.0 V window (vs. SCE) were:

$E_{1/2}(1)$= 0.417 eV (vs. SCE), $E_{1/2}(2)$= 0.568 eV (vs. SCE), $E_{1/2}(3)$= 0.884 eV (vs. SCE).

In relation to Ag/AgCl, KCl sat. electrode, 0.042 eV is added, since Ag/AgCl vs. SCE is -0.042 eV, then:

$E_{1/2}(1)$= 0.459 eV (vs. Ag/AgCl), $E_{1/2}(2)$= 0.609 eV (vs. Ag/AgCl), $E_{1/2}(3)$= 0.926 eV (vs. Ag/AgCl).

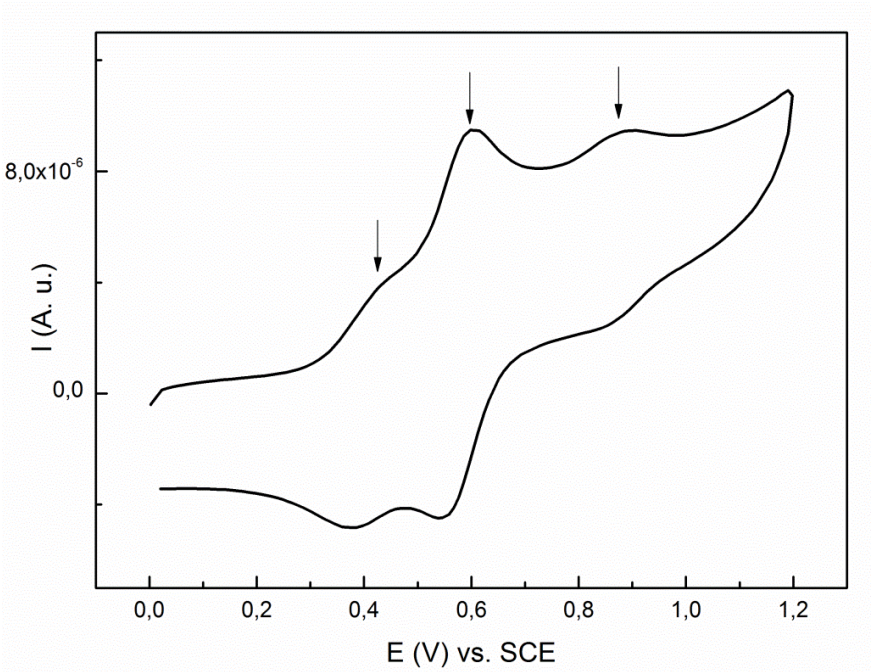

Figure III.3: Potential redox of the $Ru(dcbpy)_2(NCS)(EAFc)$ sensitizer.

The energy difference between HOMO and LUMO levels of PIMAM-OMe_{G1} (3.25 eV) is similar to the difference showed for the organic semiconductor used on hydrogel-based PV cell for Koo *et al.* [49], a system similar to our artificial leaf.

For $Ru(dcbpy)_2(NCS)(EAFc)$ it was not possible to estimate the HOMO and LUMO levels by CV since the method of calculation of these energy levels is not applicable to inorganic compounds. Our studies show that both compounds have a redox potential which is an important property to this type of systems, similar to other Ruthenium complexes previously studied [70].

IV. Conclusions and Future Work

The synthesis of photoactive components for the construction of a novel hydrogel-based solar cell system was successfully achieved. The photoactive dendrimers selected for the construction of the PV device were allyl-PIMAM-OMe_{G1} and allyl-PIMAM-OH_{G2}. These compounds have the same photoactive core (both are derived from PIMAM-OMe_{G1}) and preliminary fluorescence and CV data, acquired for the photoactive species (PIMAM-OMe_{G1} and $Ru(dcbpy)_2(NCS)(EAFc)$), show a promising potential for the desired application.

The only objective that was not fully addressed was the water solubility of the photoactive species. However, the use of an ion gel [71] as the matrix is a suitable alternative, since ionic liquids are excellent solvents for the synthesized materials. Thus, using an ion gel as the solubilizing matrix we will be able to embed all the components and create a flexible and resistant organic solar cell device.

Future work will relay in the construction and optimization of the artificial leaf using the synthesized components. To optimize the devices several studies should be performed, namely the concentration of the photoactive components and thickness of the ion gels films. After, the final system will be tested using a photoactive dendrimer-ruthenium complex,which will be synthesized through a tiol-ene reaction.

V. Bibliography

[1] D. Adam, "Industrial solvents: clean and green...but are they mean?," *Nature*, vol. 407, pp. 938–940, 2000.

[2] "Michingan Green Chemistry Clearnghouse." [Online]. Available: https://www.migreenchemistry.org/toolbox/definition-of-green-chemistry/#1. Accessed on 25/03/2015.

[3] J. C. Anastas, P. T.; Warner, *Green Chemistry: Theory and Practice*. Oxford University Press, 1998.

[4] X. Han and M. Poliakoff, "Continuous reactions in supercritical carbon dioxide: problems, solutions and possible ways forward," *Chemical Society Reviews*, vol. 41. p. 1428, 2012.

[5] R. Noyori, "Pursuing practical elegance in chemical synthesis.," *Chem. Commun. (Camb).*, pp. 1807–1811, 2005.

[6] Ž. Knez, E. Markočič, M. Leitgeb, M. Primožič, M. Knez Hrnčič, and M. Škerget, "Industrial applications of supercritical fluids: A review," *Energy*, vol. 77, pp. 235–243, Dec. 2014.

[7] M. Poliakoff and P. King, "Phenomenal fluids.," *Nature*, vol. 412, p. 125, 2001.

[8] A. R. C. Morais, A. M. da Costa Lopes, and R. Bogel-Łukasik, "Carbon Dioxide in Biomass Processing: Contributions to the Green Biorefinery Concept," *Chem. Rev.*, vol. 115, pp. 3–27, 2015.

[9] and V. K. McHugh, Mark, *Supercritical fluid extraction: principles and practice*. Elsevier, 2013.

[10] I. Pasquali, R. Bettini, and F. Giordano, "Solid-state chemistry and particle engineering with supercritical fluids in pharmaceutics," *European Journal of Pharmaceutical Sciences*, vol. 27. pp. 299–310, 2006.

[11] "The Tribal Energy and Environmental Information Clearinghouse (TEEIC)." [Online]. Available: http://teeic.indianaffairs.gov/er/carbon/carboninfo/reduce/index.htm. Accessed on 25/03/2015.

[12] "EPA United States Environmental Protection Agency." [Online]. Available: http://www.epa.gov/climatechange/ghgemissions/global.html. Accessed on 25/03/2015.

[13] "Engineered Software Knowledge Base: Modeling a Supercritical Fluid." [Online]. Available: http://kb.eng-software.com/display/ESKB/Modeling+a+Supercritical+Fluid. Accessed on 25/03/2015.

[14] P. J. Ginty, M. J. Whitaker, K. M. Shakesheff, and S. M. Howdle, "Drug delivery goes supercritical," *Materials Today*, vol. 8. pp. 42–48, 2005.

[15] P. Christian, S. M. Howdle, and D. J. Irvine, "Dispersion polymerization of methyl methacrylate in supercritical carbon dioxide with a monofunctional pseudo-graft stabilizer," *Macromolecules*, vol. 33, no. 2, pp. 237–239, 2000.

[16] T. Casimiro, A. M. Banet-Osuna, A. M. Ramos, M. N. Da Ponte, and A. Aguiar-Ricardo, "Synthesis of highly cross-linked poly(diethylene glycol dimethacrylate) microparticles in supercritical carbon dioxide," *Eur. Polym. J.*, vol. 41, no. 9, pp. 1947–1953, 2005.

[17] C. V. de Macedo, M. S. da Silva, T. Casimiro, E. J. Cabrita, and A. Aguiar-Ricardo, "Boron trifluoride catalyzed polymerisation of 2-substituted-2-oxazolines in supercritical carbon dioxide," *Green Chemistry*, vol. 9, no. 9. p. 948, 2007.

[18] A. I. Cooper, W. P. Hems, and A. B. Holmes, "Synthesis of highly cross-linked polymers in supercritical carbon dioxide by heterogeneous polymerization," *Macromolecules*, vol. 32, no. 7, pp. 2156–2166, 1999.

[19] A. R. C. Duarte, T. Casimiro, A. Aguiar-Ricardo, A. L. Simplício, and C. M. M. Duarte, "Supercritical fluid polymerisation and impregnation of molecularly imprinted polymers for drug delivery," *J. Supercrit. Fluids*, vol. 39, no. 1, pp. 102–106, 2006.

[20] R. B. Restani, P. I. Morgado, M. P. Ribeiro, I. J. Correia, A. Aguiar-Ricardo, and V. D. B. Bonifácio, "Biocompatible polyurea dendrimers with pH-dependent fluorescence," *Angew. Chemie - Int. Ed.*, vol. 51, no. 21, pp. 5162–5165, 2012.

[21] "U.S Department of Energy- Fossil Energy: How Fossil Fuels Were Formed." [Online]. Available: http://www.fe.doe.gov/education/energylessons/coal/gen_howformed.html. Accessed on 02/04/2015.
[22] "World Ocean Review: Energy." [Online]. Available: http://worldoceanreview.com/en/wor-1/energy/fossil-fuels/. Accessed on 02/04/2015.
[23] "Science: Only Zero Carbon." [Online]. Available: http://onlyzerocarbon.org/carbon_cycle.html. Accessed on 02/04/2015.
[24] "History of Fossil Fuels Usage since the Industrial Revolution." [Online]. Available: https://www.mhi-global.com/discover/earth/issue/history/history.html. Accessed on 06/04/2015.
[25] "U.S Department of Energy- Fossil Energy: A Brief Story of Coal Use." [Online]. Available: http://www.fe.doe.gov/education/energylessons/coal/coal_history.html. Accessed on 06/04/2015.
[26] REN21, "Renewables 2014: global status report."
[27] "Organization of the Petroleum Exporting Countries (OPEC)." [Online]. Available: http://www.opec.org/opec_web/en/about_us/24.htm. Accessed on 07/04/2015.
[28] "International Energy Agency (IEA)." [Online]. Available: http://www.iea.org/topics/renewables/renewablesiea/renewablesintegrationgivar/. Accessed on 07/04/2015.
[29] O. Ellabban, H. Abu-Rub, and F. Blaabjerg, "Renewable energy resources: Current status, future prospects and their enabling technology," *Renewable and Sustainable Energy Reviews*, vol. 39. pp. 748–764, 2014.
[30] S. Sista, Z. Hong, L.-M. Chen, and Y. Yang, "Tandem polymer photovoltaic cells—current status, challenges and future outlook," *Energy Environ. Sci.*, vol. 4, no. 5, p. 1606, 2011.
[31] T. Saga, "Advances in crystalline silicon solar cell technology for industrial mass production," *NPG Asia Materials*, vol. 2, no. 3. pp. 96–102, 2010.
[32] S. Honsberg, C.; Bowden, "A collection of resources for the photovoltaic cells." [Online]. Available: http://www.pveducation.org/.
[33] A. M. Bagher, "Comparison of organic solar cells and inorganic solar cells 2 . How Do Organic Solar Cells Work," *Int. J. Renew. Sustain. Energy*, vol. 3, no. 3, pp. 53–58, 2014.
[34] American Chemical Society (ACS), "Chem Matters Online: How a Solar Cell Works." [Online]. Available: https://www.acs.org/content/acs/en/education/resources/highschool/chemmatters/past-issues/archive-2013-2014/how-a-solar-cell-works.html?cq_ck=1396892718960. Accessed on 08/04/2015.
[35] R. W. Miles, G. Zoppi, and I. Forbes, "Inorganic photovoltaic cells," *Mater. Today*, vol. 10, no. 11, pp. 20–27, Nov. 2007.
[36] Fraunhofer, "Photovoltaics Report."
[37] A. Kolodziej, "Staebler-Wronski effect in amorphous silicon and its alloys," *Opto-Electronics Rev.*, vol. 12, no. 1, pp. 21–32, 2004.
[38] M. Cardona, Peter YU, *Fundamentals of Semiconductors:Physics and Materials Properties*. Springer Science & Business Media, 2010.
[39] J.-M. Nunzi, "Organic photovoltaic materials and devices," *Comptes Rendus Phys.*, vol. 3, no. 4, pp. 523–542, Jan. 2002.
[40] S. Günes, H. Neugebauer, and N. S. Sariciftci, "Conjugated polymer-based organic solar cells," *Chemical Reviews*, vol. 107, no. 4. pp. 1324–1338, 2007.
[41] J. Nelson, "Organic photovoltaic films," *Curr. Opin. Solid State Mater. Sci.*, vol. 6, no. 1, pp. 87–95, Feb. 2002.
[42] M. W. Rowell, M. A. Topinka, M. D. McGehee, H. J. Prall, G. Dennler, N. S. Sariciftci, L. Hu, and G. Gruner, "Organic solar cells with carbon nanotube network electrodes," *Appl. Phys. Lett.*, vol. 88, no. 23, 2006.
[43] M. D. McGehee and M. A. Topinka, "Solar cells: Pictures from the blended zone.," *Nature materials*, vol. 5, no. 9. pp. 675–676, 2006.

[44] T. Ameri, G. Dennler, C. Lungenschmied, and C. J. Brabec, “Organic tandem solar cells: A review,” *Energy & Environmental Science*, vol. 2, no. 4. p. 347, 2009.
[45] A. Hadipour, B. De Boer, J. Wildeman, F. B. Kooistra, J. C. Hummelen, M. G. R. Turbiez, M. M. Wienk, R. A. J. Janssen, and P. W. M. Blom, “Solution-processed organic tandem solar cells,” *Adv. Funct. Mater.*, vol. 16, no. 14, pp. 1897–1903, 2006.
[46] J. Xue, S. Uchida, B. P. Rand, and S. R. Forrest, “Asymmetric tandem organic photovoltaic cells with hybrid planar-mixed molecular heterojunctions,” *Appl. Phys. Lett.*, vol. 85, no. 23, pp. 5757–5759, 2004.
[47] B. Maennig, J. Drechsel, D. Gebeyehu, P. Simon, F. Kozlowski, A. Werner, F. Li, S. Grundmann, S. Sonntag, M. Koch, K. Leo, M. Pfeiffer, H. Hoppe, D. Meissner, N. S. Sariciftci, I. Riedel, V. Dyakonov, and J. Parisi, “Organic p-i-n solar cells,” *Appl. Phys. A Mater. Sci. Process.*, vol. 79, no. 1, pp. 1–14, 2004.
[48] M. Wright and A. Uddin, “Organic—inorganic hybrid solar cells: A comparative review,” *Sol. Energy Mater. Sol. Cells*, vol. 107, pp. 87–111, Dec. 2012.
[49] H.-J. Koo, S. T. Chang, J. M. Slocik, R. R. Naik, and O. D. Velev, “Aqueous soft matter based photovoltaic devices,” *J. Mater. Chem.*, vol. 21, no. 1, p. 72, 2011.
[50] W. H. Lai, Y. H. Su, L. G. Teoh, and M. H. Hon, “Commercial and natural dyes as photosensitizers for a water-based dye-sensitized solar cell loaded with gold nanoparticles,” *J. Photochem. Photobiol. A Chem.*, vol. 195, no. 2–3, pp. 307–313, 2008.
[51] N. Terasaki, N. Yamamoto, T. Hiraga, Y. Yamanoi, T. Yonezawa, H. Nishihara, T. Ohmori, M. Sakai, M. Fujii, A. Tohri, M. Iwai, Y. Inoue, S. Yoneyama, M. Minakata, and I. Enami, “Plugging a molecular wire into photosystem I: Reconstitution of the photoelectric conversion system on a gold electrode,” *Angew. Chemie - Int. Ed.*, vol. 48, no. 9, pp. 1585–1587, 2009.
[52] P. N. Ciesielski, A. M. Scott, C. J. Faulkner, B. J. Berron, D. E. Cliffel, and G. K. Jennings, “Functionalized nanoporous gold leaf electrode films for the immobilization of photosystem I,” *ACS Nano*, vol. 2, no. 12, pp. 2465–2472, 2008.
[53] T. N. Murakami, H. Saito, S. Uegusa, N. Kawashima, and T. Miyasaka, “Water-based Dye-sensitized Solar Cells: Interfacial Activation of TiO2 Mesopores in Contact with Aqueous Electrolyte for Efficiency Development,” *Chemistry Letters*, vol. 32, no. 12. pp. 1154–1155, 2003.
[54] A. Harriman, M. A. H. Alamiry, J. P. Hagon, D. Hablot, and R. Ziessel, “Through-space electronic energy transfer across proximal molecular dyads.,” *Angew. Chem. Int. Ed. Engl.*, vol. 52, no. 26, pp. 6611–5, Jun. 2013.
[55] J. J. Concepcion, R. L. House, J. M. Papanikolas, and T. J. Meyer, “Chemical approaches to artificial photosynthesis.,” *Proc. Natl. Acad. Sci. U. S. A.*, vol. 109, no. 39, pp. 15560–4, Sep. 2012.
[56] D. Astruc, “Electron-transfer processes in dendrimers and their implication in biology, catalysis, sensing and nanotechnology.,” *Nat. Chem.*, vol. 4, no. 4, pp. 255–67, Apr. 2012.
[57] K. . Iida and Y. Kawamura, “Organic compound, Charge-transporting material, composition for change-transporting material and organic electroluminescence device.”
[58] H. Mohindra Chawla and M. Pathak, “Dye sensitized photooxygenation of imidazolin-2-ones,” *Tetrahedron*, vol. 46, no. 4, pp. 1331–1342, Jan. 1990.
[59] E. A. Medlycott and G. S. Hanan, “Designing tridentate ligands for ruthenium(II) complexes with prolonged room temperature luminescence lifetimes.,” *Chem. Soc. Rev.*, vol. 34, no. 2, pp. 133–42, Feb. 2005.
[60] Y. Ahn, Y. Jang, N. Selvapalam, G. Yun, and K. Kim, “Supramolecular velcro for reversible underwater adhesion.,” *Angew. Chem. Int. Ed. Engl.*, vol. 52, no. 11, pp. 3140–4, Mar. 2013.
[61] W. S. Jeon, K. Moon, S. H. Park, H. Chun, Y. H. Ko, J. Y. Lee, E. S. Lee, S. Samal, N. Selvapalam, M. V Rekharsky, V. Sindelar, D. Sobransingh, Y. Inoue, A. E. Kaifer, and K. Kim, “Complexation of ferrocene derivatives by the cucurbit[7]uril host: a comparative study of the cucurbituril and cyclodextrin host families.,” *J. Am. Chem. Soc.*, vol. 127, no. 37, pp. 12984–9, Sep. 2005.

[62] C. M. Cardona, T. D. McCarley, and A. E. Kaifer, “Synthesis, Electrochemistry, and Interactions with β-Cyclodextrin of Dendrimers Containing a Single Ferrocene Subunit Located ‘Off-Center,’” *J. Org. Chem.*, vol. 65, no. 6, pp. 1857–1864, Mar. 2000.

[63] J. M. Casas-Solvas, E. Ortiz-Salmerón, I. Fernández, L. García-Fuentes, F. Santoyo-González, and A. Vargas-Berenguel, “Ferrocene-beta-cyclodextrin conjugates: synthesis, supramolecular behavior, and use as electrochemical sensors.,” *Chemistry*, vol. 15, no. 33, pp. 8146–62, Aug. 2009.

[64] A. Gadelle and J. Defaye, “Selective Halogenation at Primary Positions of Cyclomaltooligosaccharides and a Synthesis of Per-3,6-anhydro Cyclomaltooligosaccharides,” *Angew. Chemie Int. Ed. English*, vol. 30, no. 1, pp. 78–80, Jan. 1991.

[65] M. T. Rojas, R. Koeniger, J. F. Stoddart, and A. E. Kaifer, “Supported Monolayers Containing Preformed Binding Sites. Synthesis and Interfacial Binding Properties of a Thiolated .beta.-Cyclodextrin Derivative,” *J. Am. Chem. Soc.*, vol. 117, no. 1, pp. 336–343, Jan. 1995.

[66] N. C. Tice, S. Parkin, and J. P. Selegue, “Synthesis, characterization and crystal structures of boron-containing intermediates in the reductive amination of ferrocenecarboxaldehyde to a bis(ferrocenylmethyl) amine,” *J. Organomet. Chem.*, vol. 692, pp. 791–800, 2007.

[67] D. Andrianina Ralambomanana, D. Razafimahefa-Ramilison, A. C. Rakotohova, J. Maugein, and L. Pélinski, “Synthesis and antitubercular activity of ferrocenyl diaminoalcohols and diamines,” *Bioorganic Med. Chem.*, vol. 16, pp. 9546–9553, 2008.

[68] A. Harada and S. Takahashi, “Preparation and properties of cyclodextrin inclusion compounds of organometallic complexes. Ferrocene inclusion compounds,” *J. Incl. Phenom.*, vol. 2, no. 3–4, pp. 791–798, 1984.

[69] A. M. Bond, K. B. Oldham, and G. A. Snook, “Use of the ferrocene oxidation process to provide both reference electrode potential calibration and a simple measurement (via semiintegration) of the uncompensated resistance in cyclic voltammetric studies in high-resistence organic solvents,” *Anal. Chem.*, vol. 72, no. 15, pp. 3492–3496, 2000.

[70] S. H. Wu, J. J. Shen, J. Yao, and Y. W. Zhong, “Asymmetric mixed-valence complexes that consist of cyclometalated ruthenium and ferrocene: Synthesis, characterization, and electronic-coupling studies,” *Chem. - An Asian J.*, vol. 8, no. 1, pp. 138–147, 2013.

[71] P. Vidinha, N. M. T. Lourenço, C. Pinheiro, A. R. Brás, T. Carvalho, T. Santos-Silva, A. Mukhopadhyay, M. J. Romão, J. Parola, M. Dionisio, J. M. S. Cabral, C. A. M. Afonso, and S. Barreiros, “Ion jelly: a tailor-made conducting material for smart electrochemical devices.,” *Chem. Commun. (Camb).*, no. 44, pp. 5842–5844, 2008.

VI. Appendix

a. Appendix I

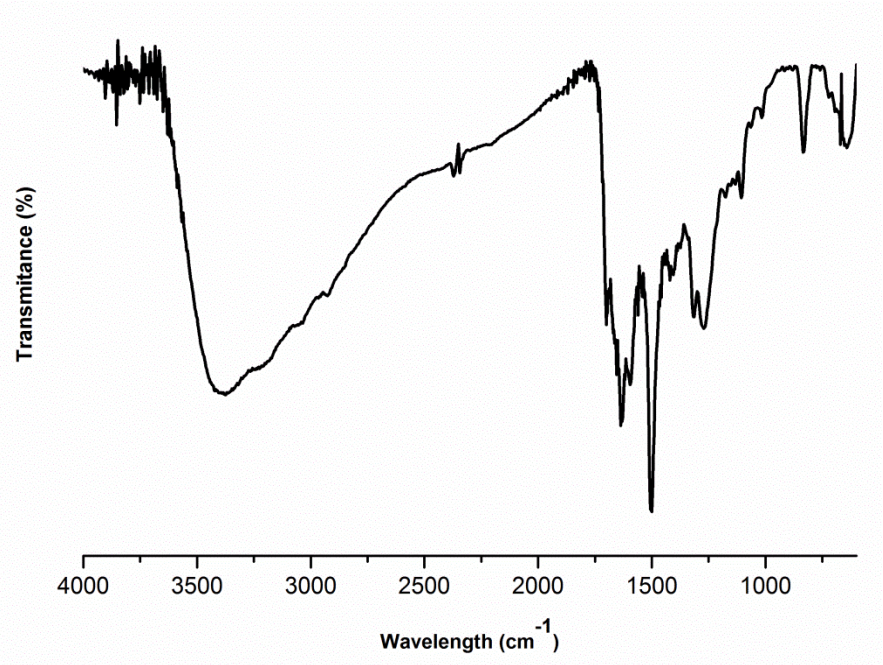

Figure VI.1: FTIR spectrum of the $PURAM_{G1}$ dendrimer in KBr.

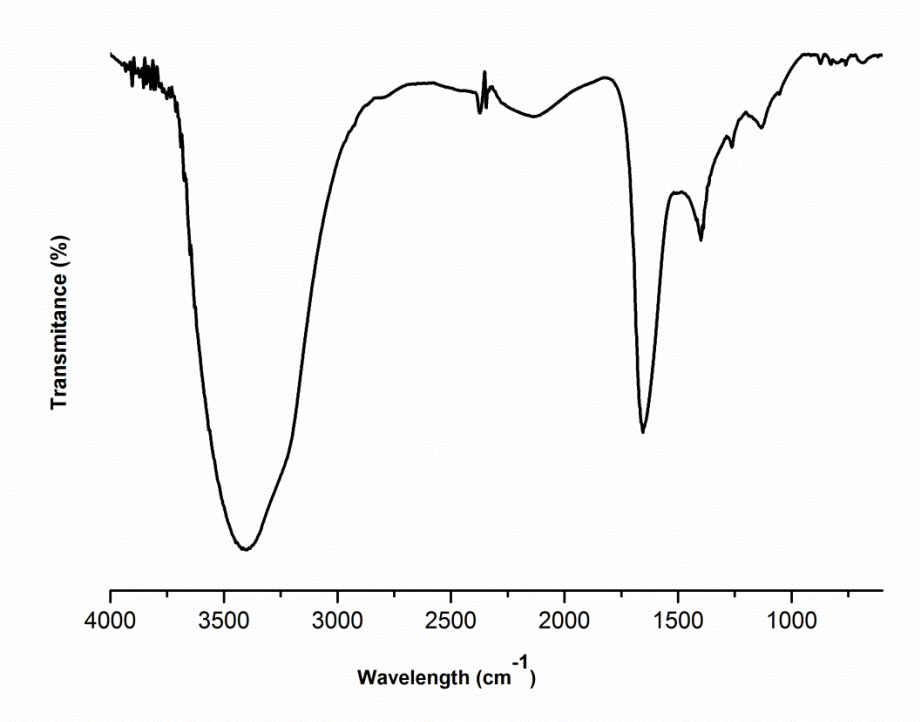

Figure VI.2: FTIR spectrum of the $PURAP_{G1}$ dendrimer in NaCl film.

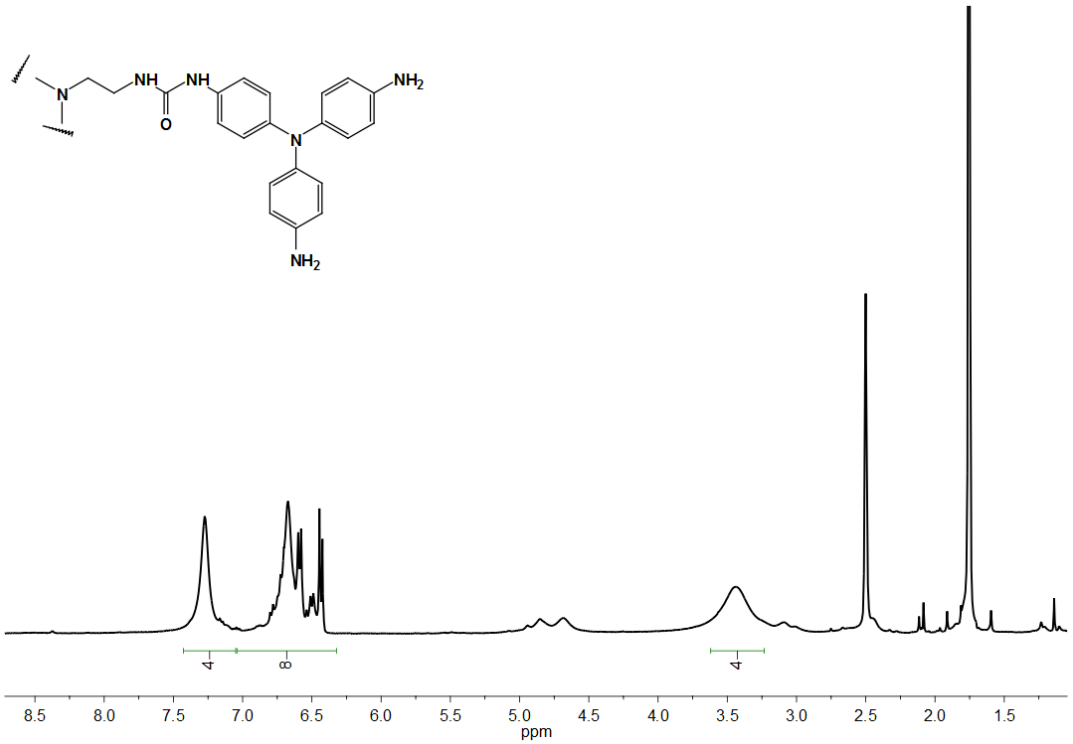

Figure VI.3: ^{1}H NMR spectrum of the PURAP$_{G1}$ dendrimer in DMSO-*d6*.

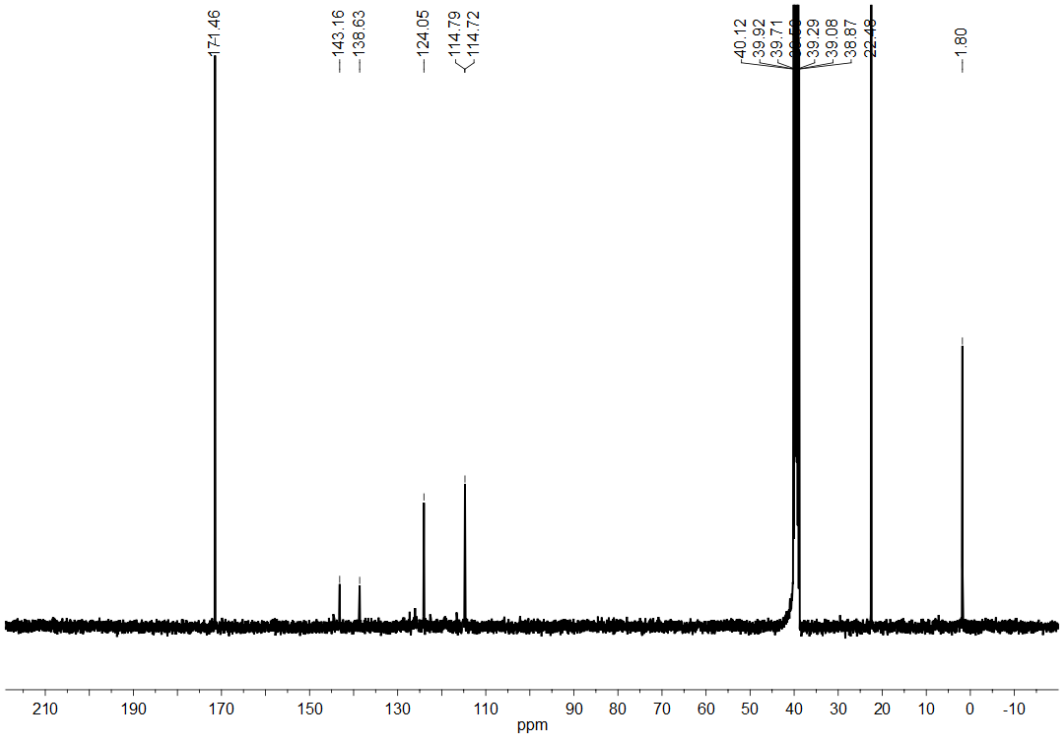

Figure VI.4: ^{13}C NMR spectrum of the PURAP$_{G1}$ dendrimer in DMSO-*d6*.

b. Appendix II

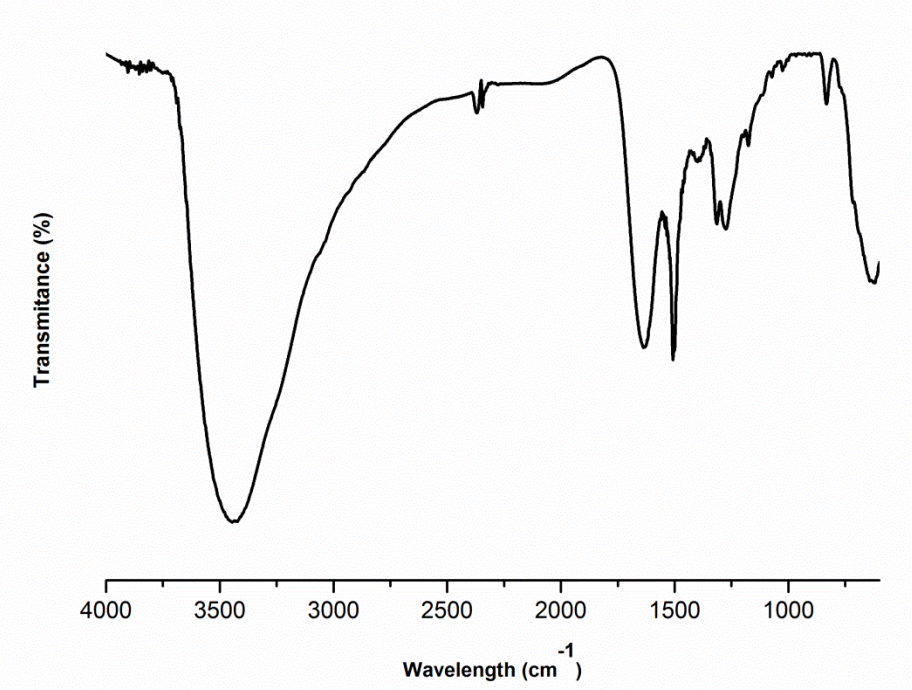

Figure VI.5: FTIR spectrum of the $PIMAM_{G1}$ dendrimer in KBr.

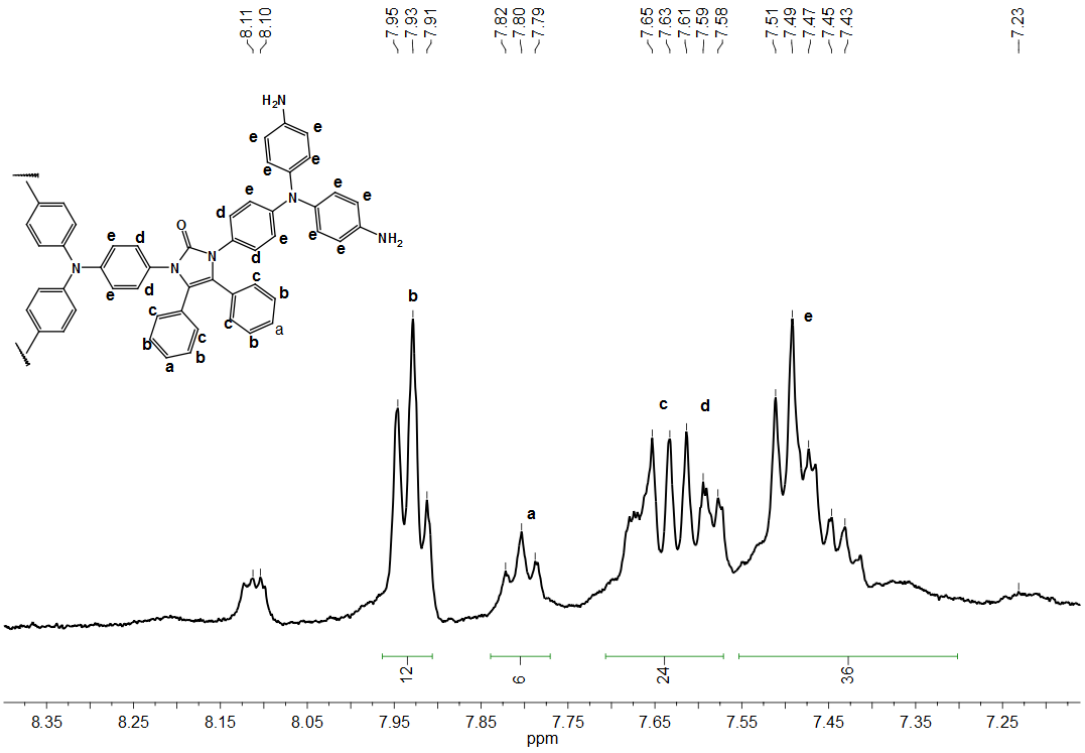

Figure VI.6: ^{1}H NMR spectrum of the $PIMAM_{G1}$ dendrimer in DMSO-*d6*.

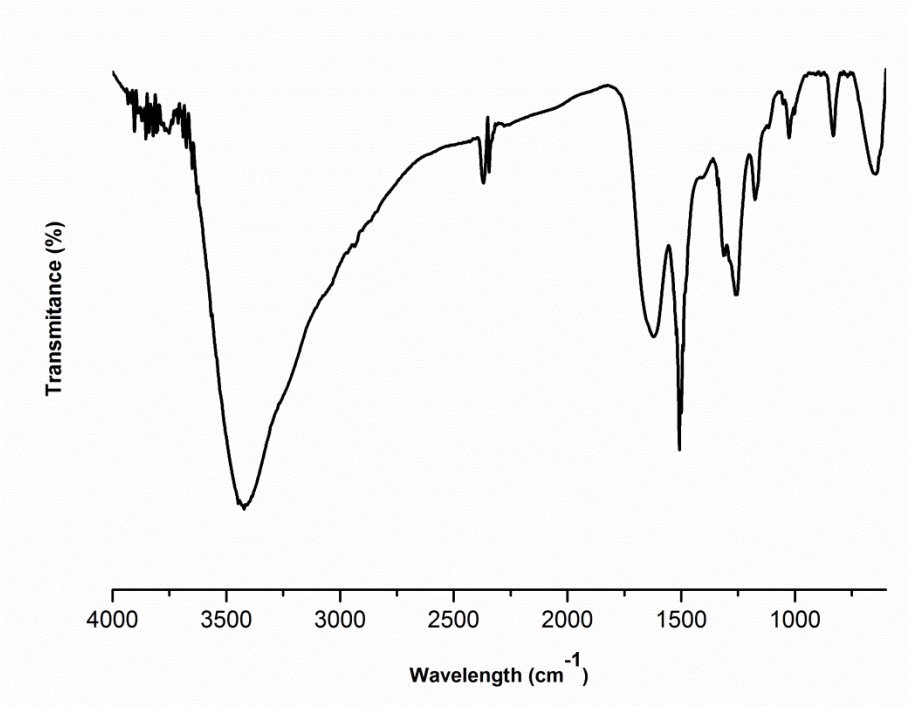

Figure VI.7: FTIR spectrum of the PIMAM-OMe$_{G1}$ dendrimer in KBr.

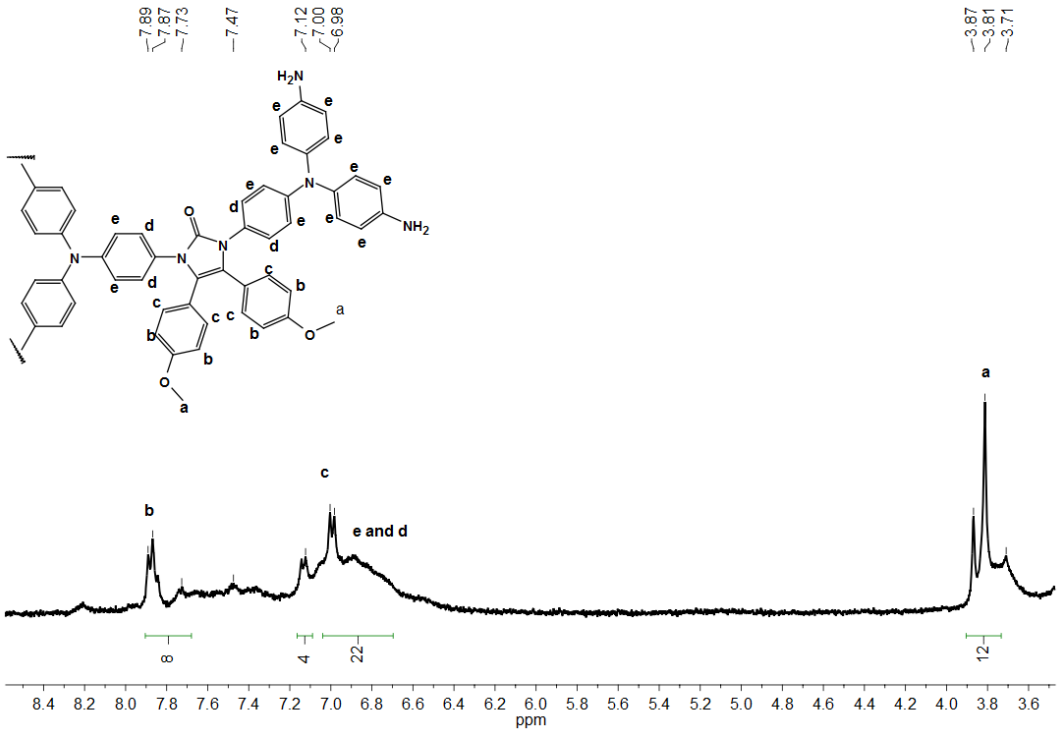

Figure VI.8: ^{1}H NMR spectrum of the PIMAM-OMe$_{G1}$ dendrimer in DMSO-*d6*.

c. Appendix III

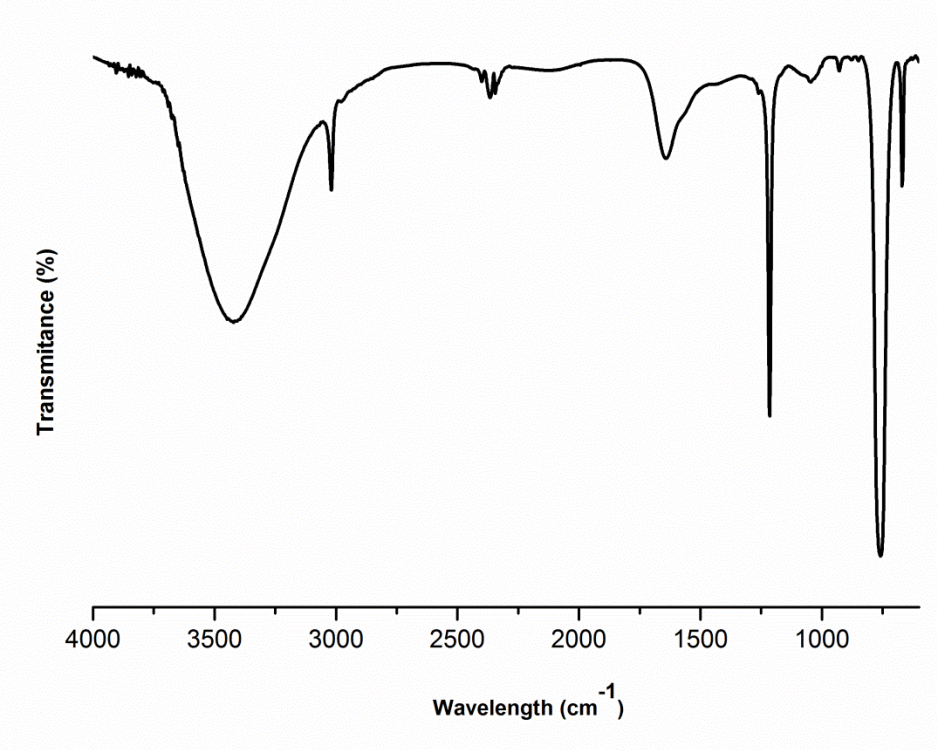

Figure VI.9: FTIR spectrum of the $PIMAM_{G2}$ dendrimer in KBr.

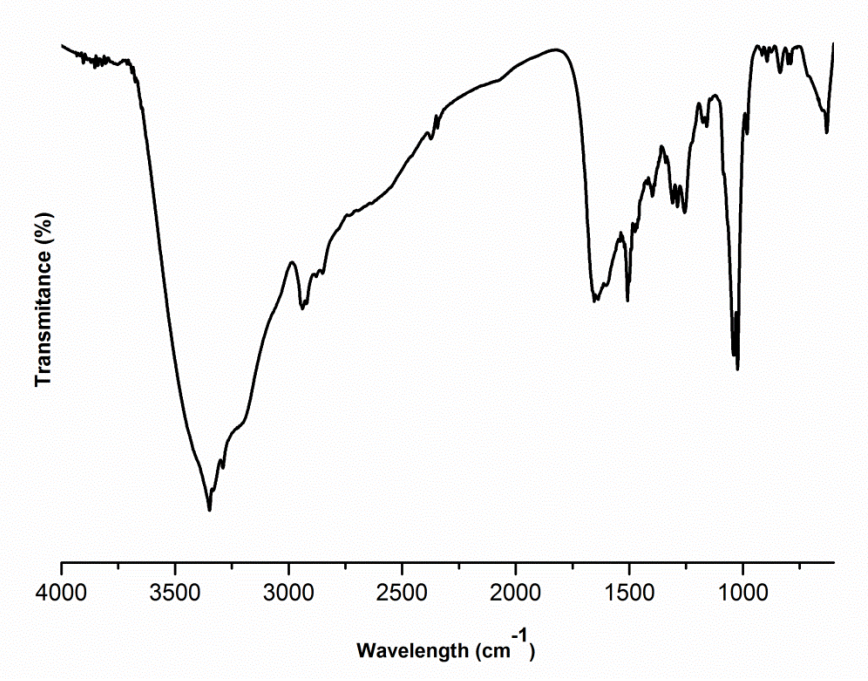

Figure VI.10: FTIR spectrum of the PIMAM-OH_{G2} dendrimer in KBr.

d. Appendix IV

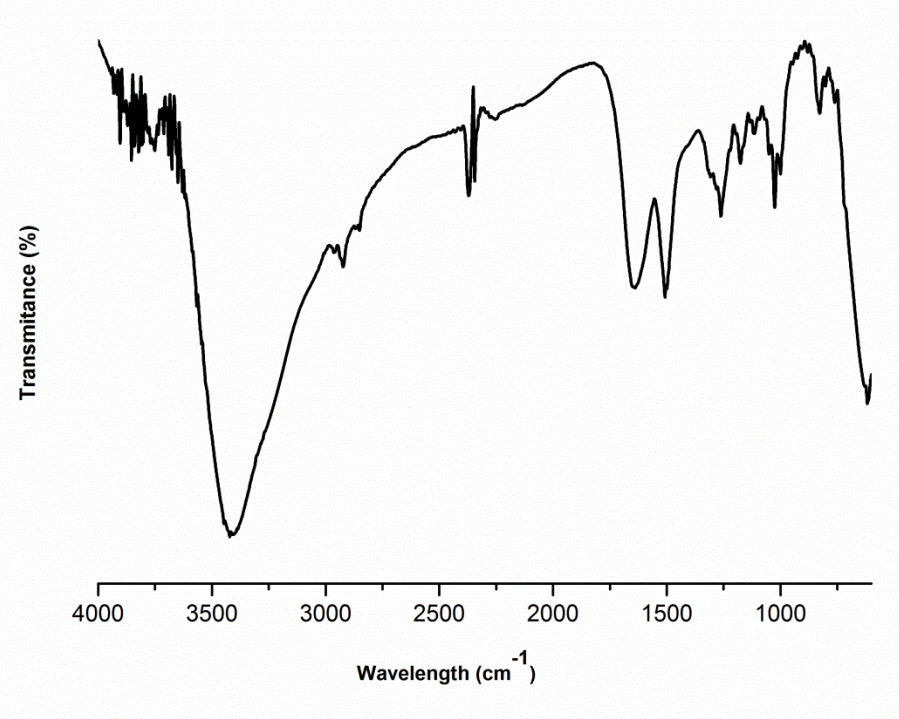

Figure VI.11: FTIR spectrum of the allyl-PIMAM-OH_{G2} dendrimer in KBr.

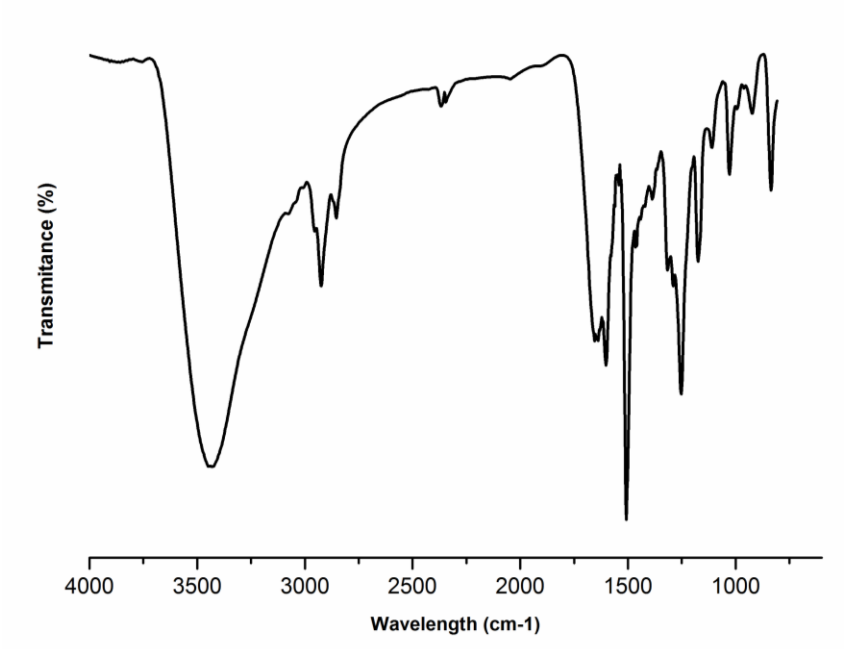

Figure VI.12: FTIR spectrum of the allyl-$PIMAM_{G2}$ in KBr.

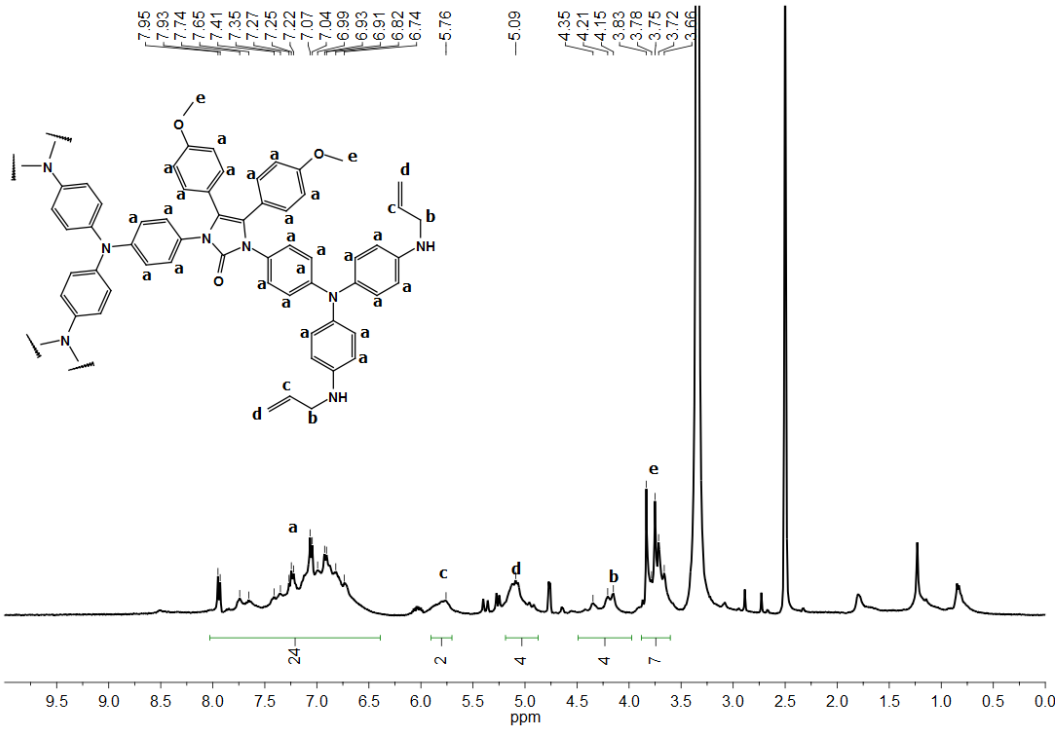

Figure VI.13: ^{1}H NMR spectrum of the allyl-PIMAM-OMe$_{G1}$ dendrimer in in DMSO-*d6*.

e. Appendix V

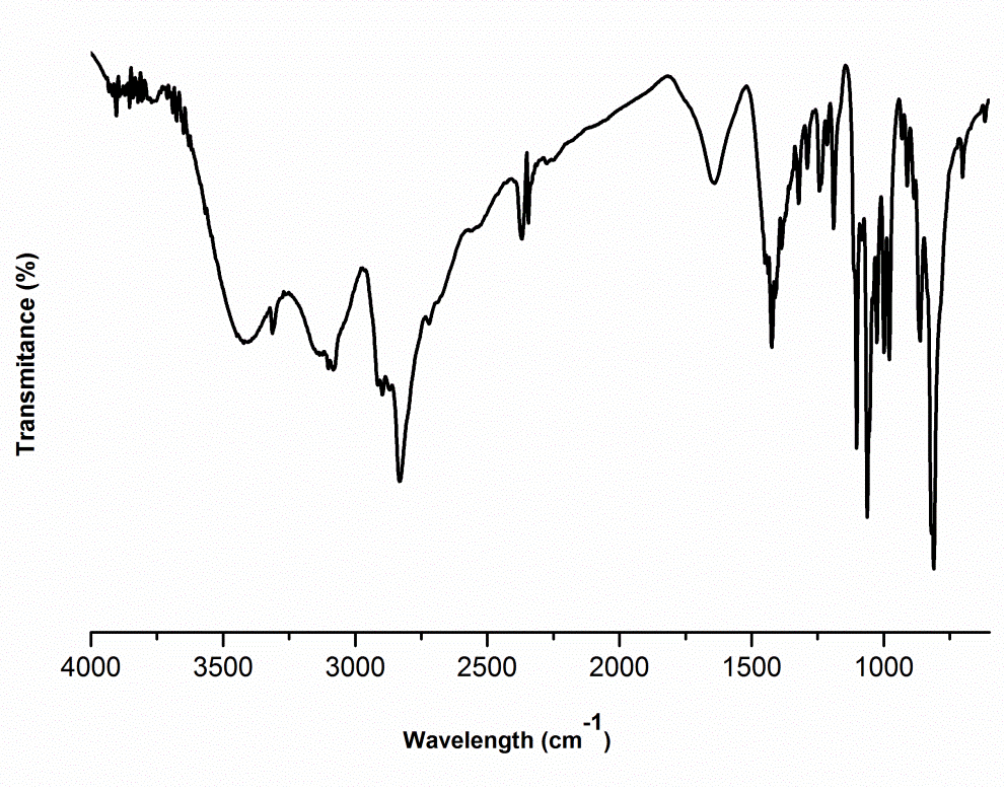

Figure VI.14: FTIR spectrum of EAFc in KBr.

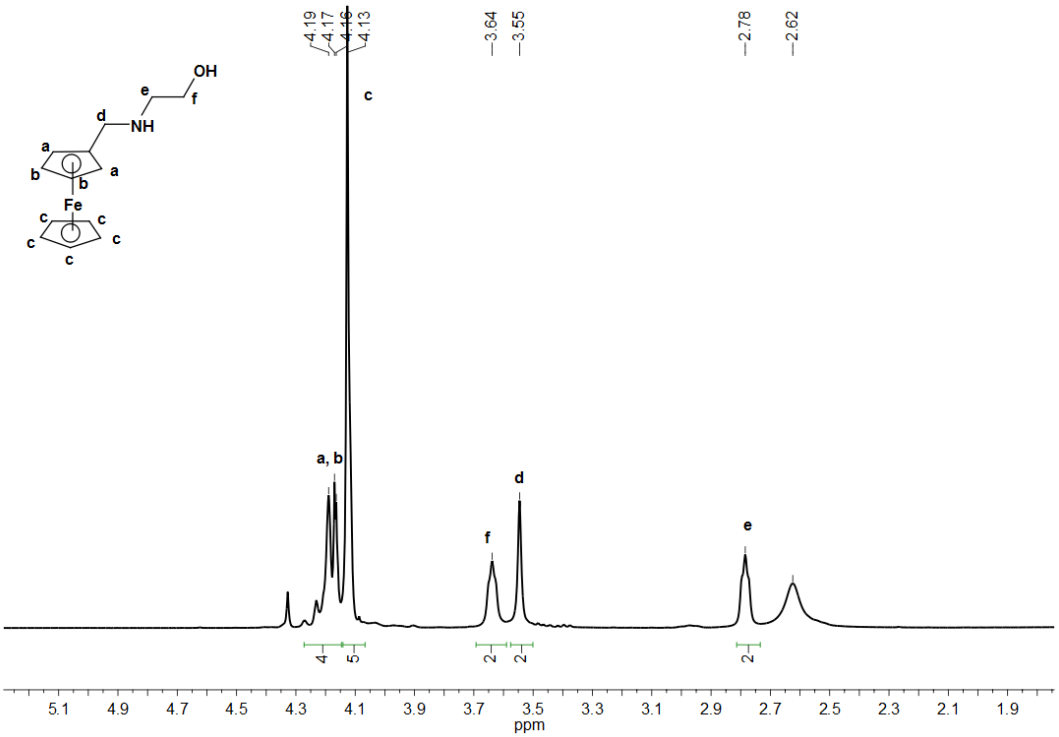

Figure VI.15: ^{1}H NMR spectrum of EAFc in $CDCl_3$.

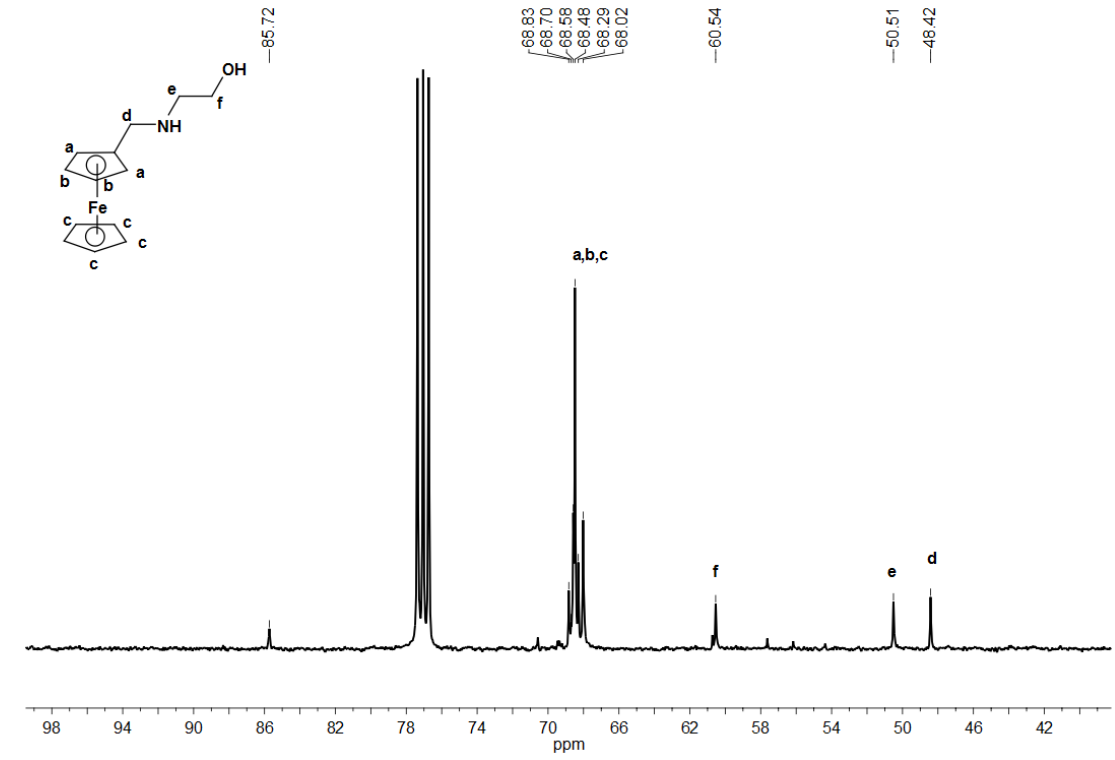

Figure VI.16: ^{13}C NMR spectrum of EAFc in $CDCl_3$.

f. Appendix VI

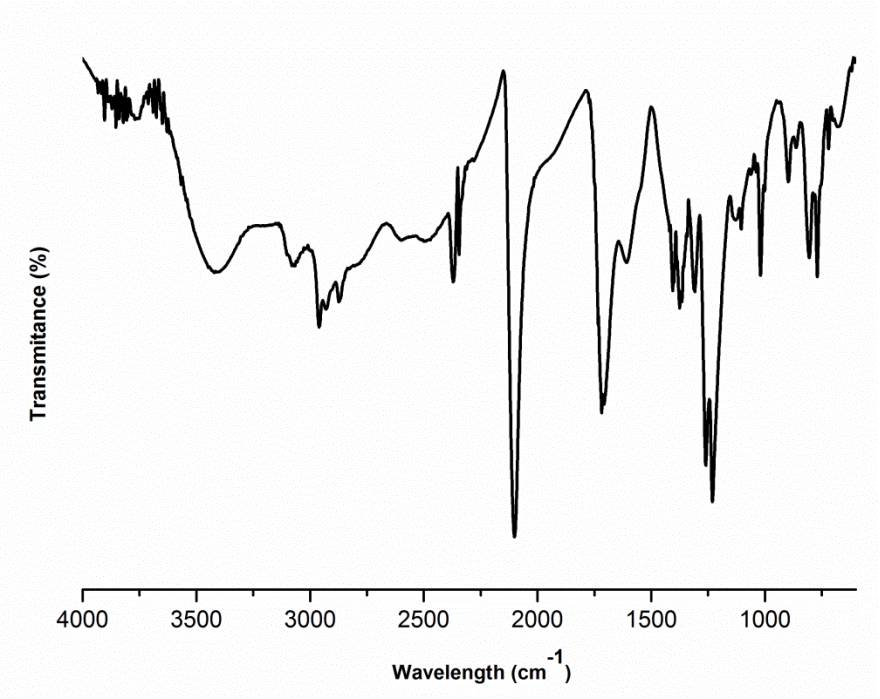

Figure VI.17: FTIR spectrum of the $Ru(dcbpy)_2(NCS)(EAFc)$ sensitizer in KBr.

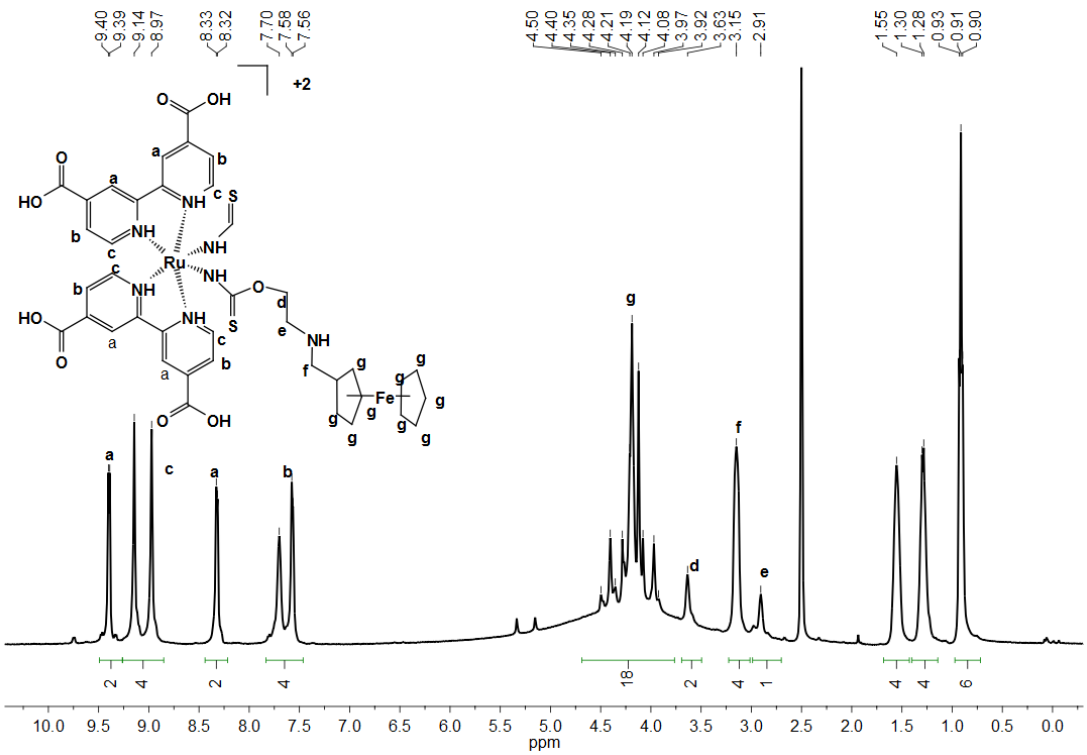

Figure VI.18: ^1H NMR spectrum of the $Ru(dcbpy)_2(NCS)(EAFc)$ sensitizer in in DMSO-*d6*.

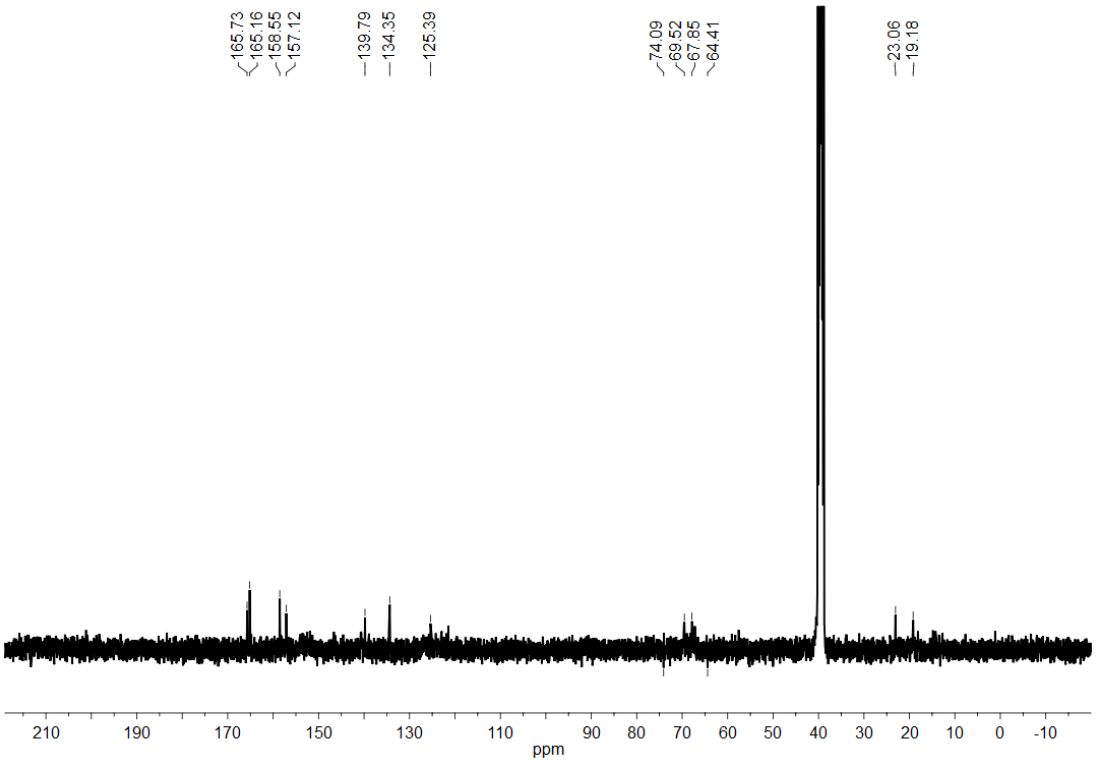

Figure VI.19: ^{13}C NMR spectrum of $Ru(dcbpy)_2(NCS)(EAFc)$ sensitizer in DMSO-*d6*.

g. Appendix VII

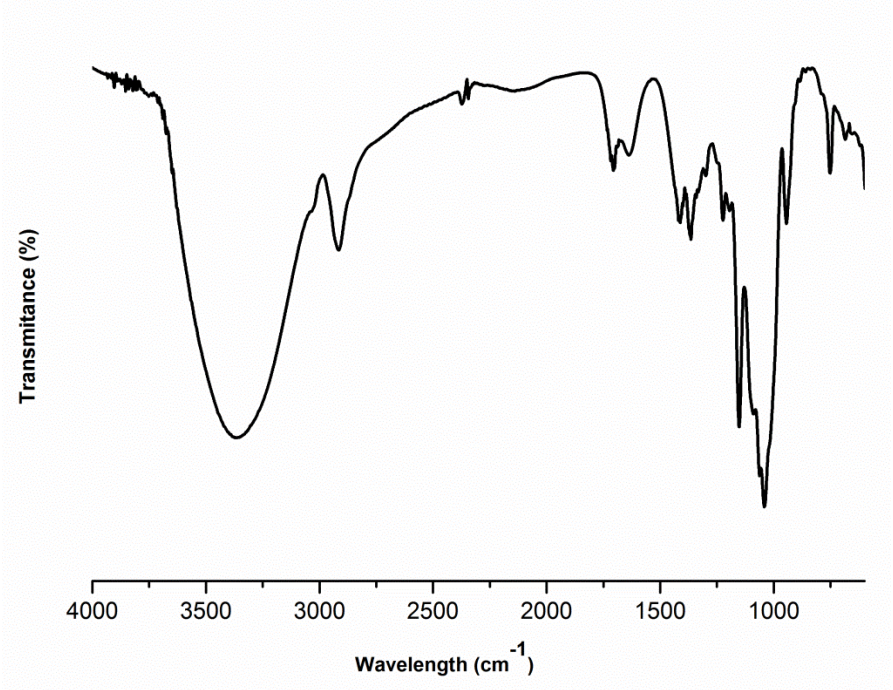

Figure VI.20: FTIR spectrum of per-6-iodo-β-cyclodextrin in KBr.

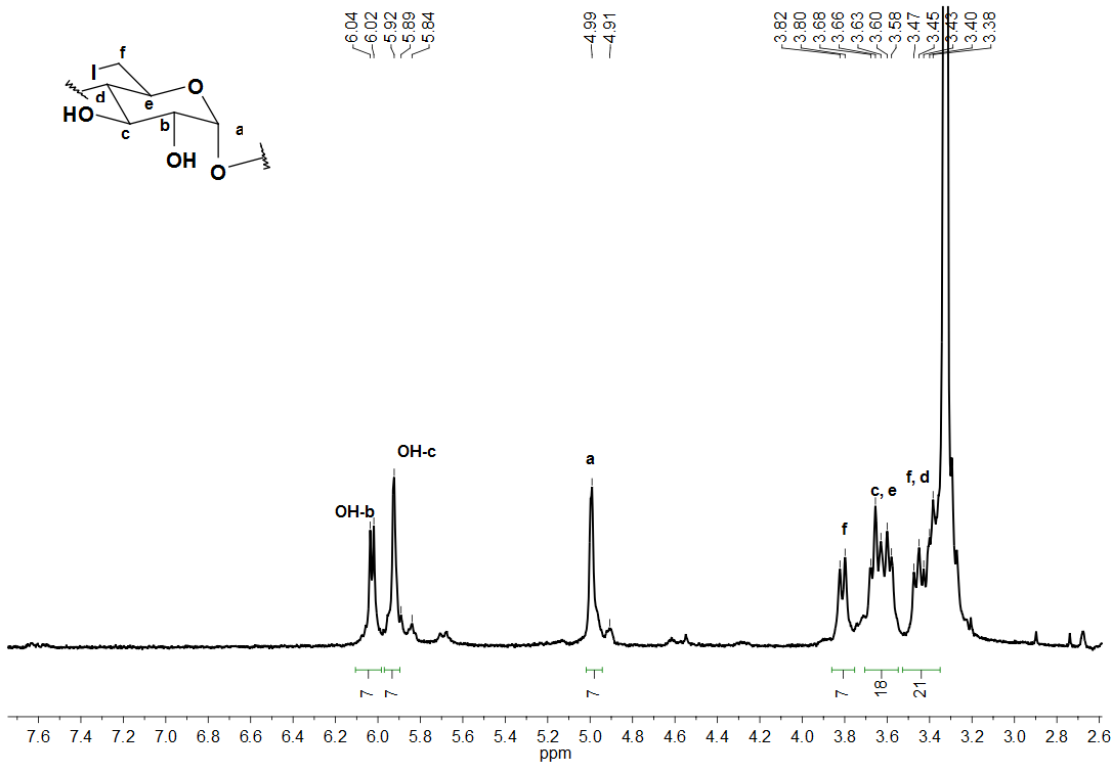

Figure VI.21: [1]H NMR spectrum of per-6-iodo-β-cyclodextrin in DMSO-*d6*.

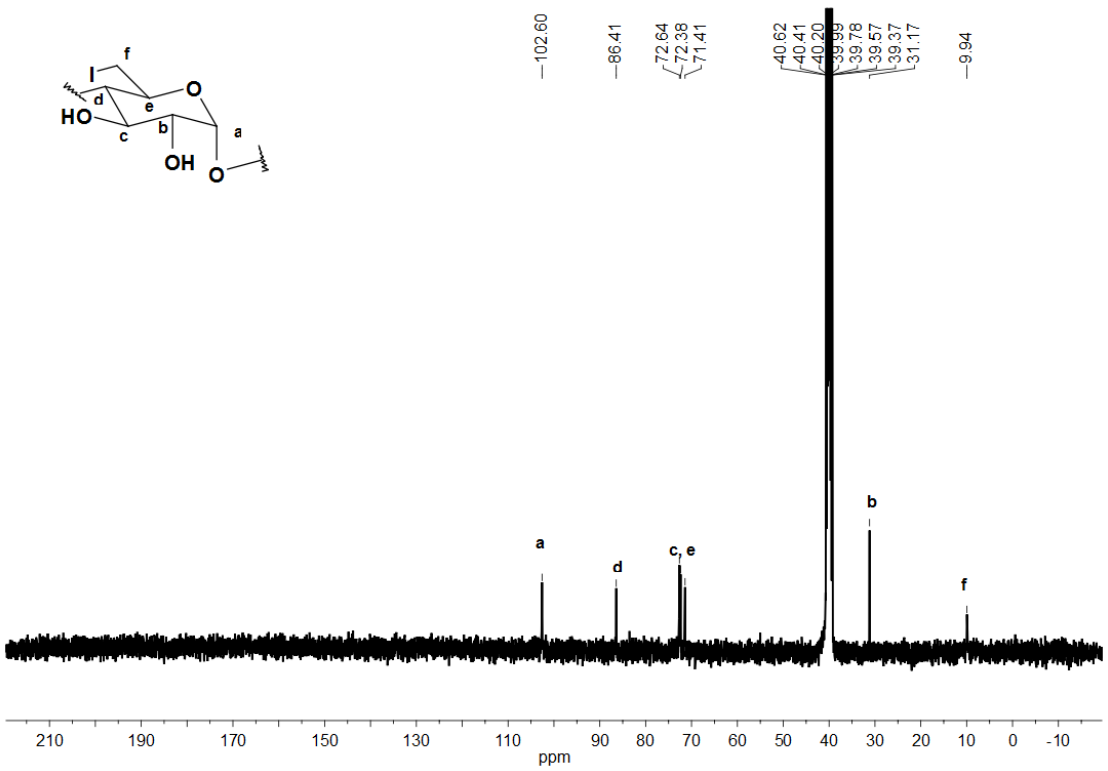

Figure VI.22: [13]C NMR spectrum of per-6-iodo-β-cyclodextrin in DMSO-*d6*.

h. Appendix VIII

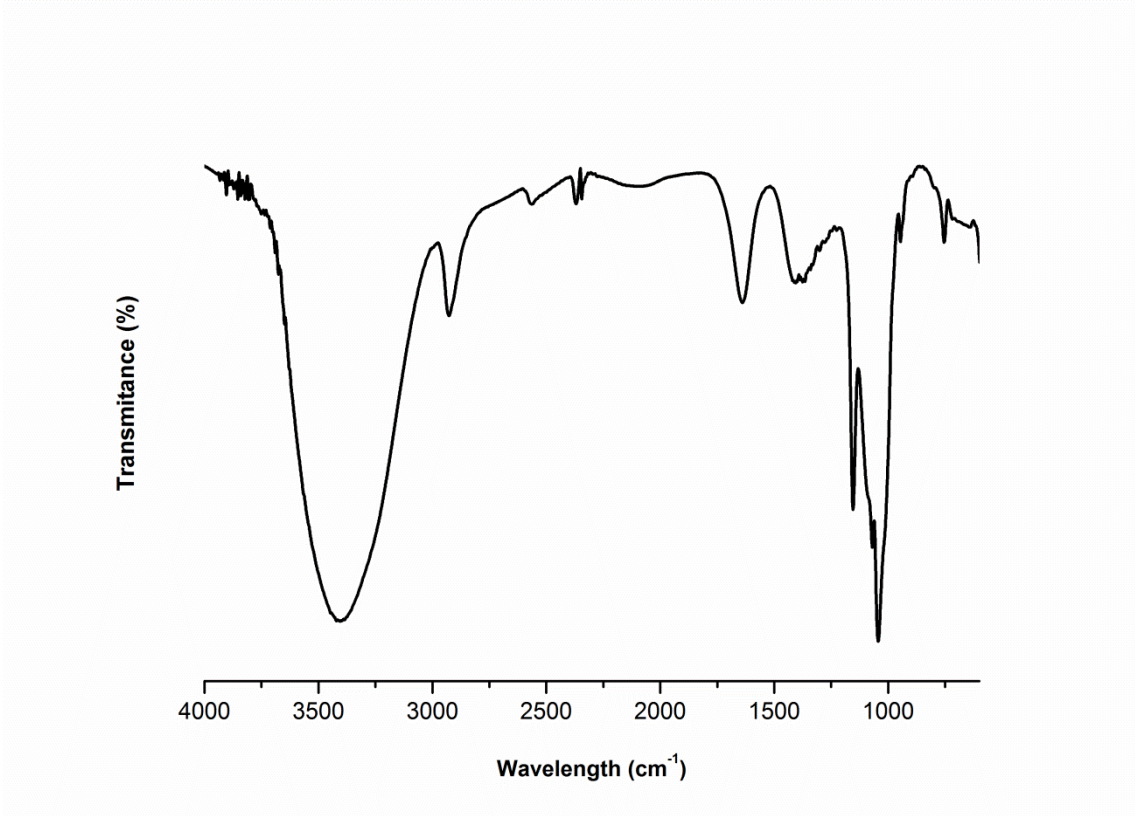

Figure VI.23: FTIR spectrum of per-6-thio-β-cyclodextrin in KBr.

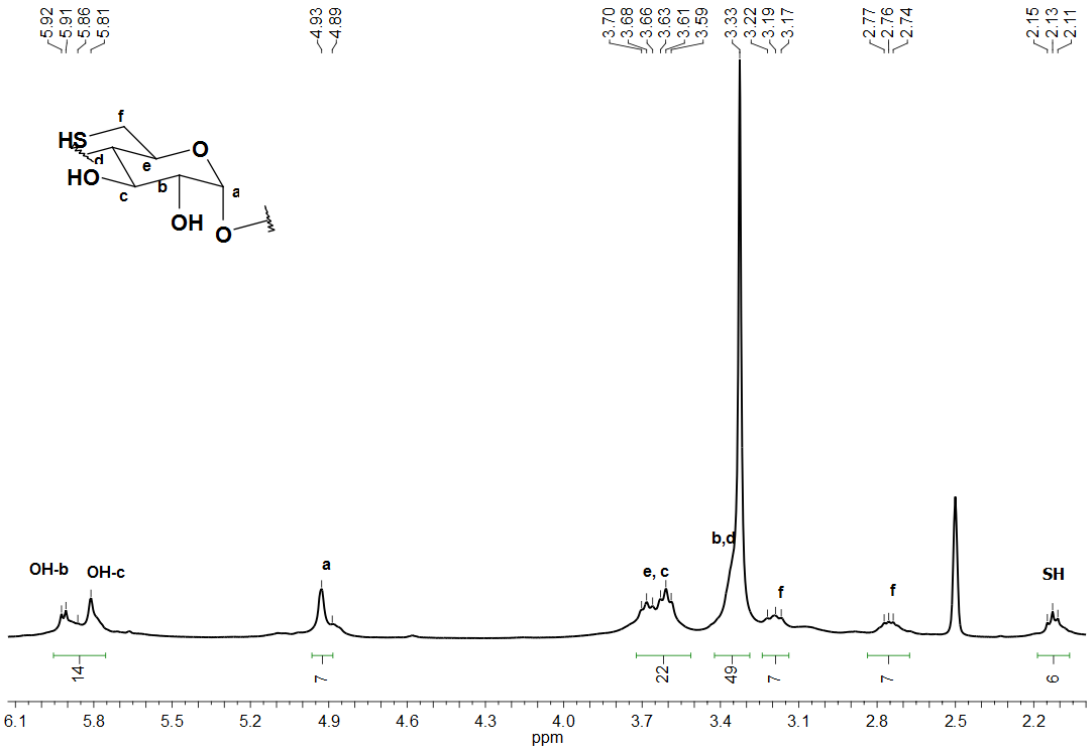

Figure VI.24: ^{1}H NMR spectrum of per-6-thio-β-cyclodextrin in DMSO-*d6*.

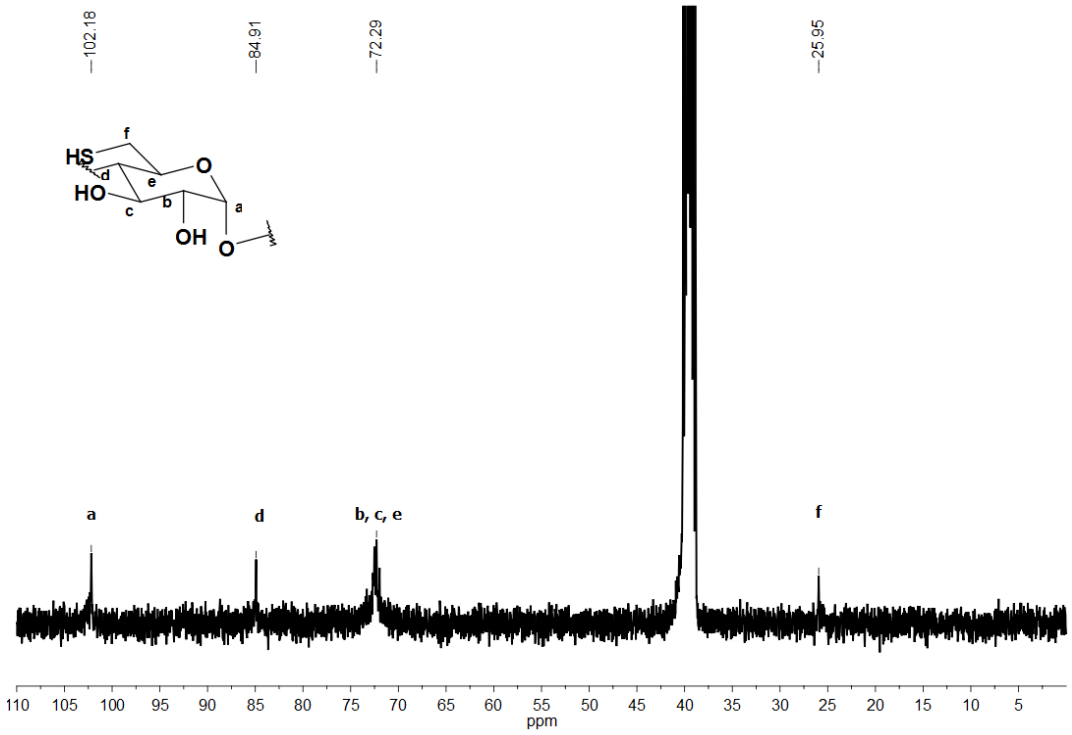

Figure VI.25: ^{13}C NMR spectrum of per-6-thio-β-cyclodextrin in DMSO-*d6*.